Unravelling specific diet and gut microbial contributions to inflammatory bowel disease

Gabriel Vasconcelos Pereira[1,#], Marie Boudaud[2,#], Mathis Wolter[2,3], Celeste Alexander[1], Alessandro De Sciscio[2], Erica. T Grant[2,3], Bruno Caetano Trindade, Shaleni Singh[1], Austin Campbell[1], Nicholas A. Pudlo, Stéphanie Willieme[2], Sophie Craig[2], Kwi Kim[1], Trisha Denike-Duval[1], Lucy Kennedy[1], Thomas M. Schmidt[1], Grace Chen[1], Kathryn Eaton[1], Mahesh S. Desai[2,4,$,*], Eric C. Martens[1,$,§,*]

Affiliations:

[1]Department of Microbiology and Immunology, University of Michigan Medical School, Ann Arbor, Michigan, USA

[2]Department of Infection and Immunity, Luxembourg Institute of Health, 4354 Esch-sur-Alzette, Luxembourg

[3]Faculty of Science, Technology and Medicine, University of Luxembourg, 4365 Esch-sur-Alzette, Luxembourg

[4]Odense Research Center for Anaphylaxis, Department of Dermatology and Allergy Center, Odense University Hospital, University of Southern Denmark, 5000 Odense, Denmark

[#]Authors contributed equally

*Correspondence to: emartens@umich.edu, mahesh.desai@lih.lu

[§]Lead author

[$]Senior authors

Summary

Inflammatory bowel disease (IBD) is a chronic condition characterized by periods of spontaneous intestinal inflammation and is increasing in industrialized populations. Combined with host genetic predisposition, both diet and gut bacteria are thought to be prominent environmental features contributing to IBD, but little is known about the precise mechanisms. We show that low dietary fiber promotes bacterial erosion of the protective colonic mucus layer, leading to lethal colitis in interleukin-10-deficient mice. This diet-induced inflammation is specifically driven by mucin-degrading bacteria-mediated Th1 immune responses and is preceded by expansion of natural killer T cells and reduced immunoglobulin A coating of specific bacterial species. Low fiber, exclusive enteral nutrition reduced disease in part by increasing bacterial production of the metabolite isobutyrate, which was dependent on the presence of soy protein in the diet. Our results highlight a mechanistic framework to unravel the complex web of potentially opposing diet, host and microbial factors that combine to influence IBD development.

54 **Introduction**

55 Inflammatory bowel disease (IBD) occurs in people with underlying genetic variations
56 that cause inappropriate immunological responses to intestinal antigens, especially ordinarily
57 non-harmful symbiotic gut microbes (Shan et al., 2021). Despite identification of hundreds of
58 IBD-associated genetic polymorphisms (Mirkov et al., 2017), the precise mechanisms through
59 which IBD develops have not yet been determined. Even when predisposing genetics exist, IBD
60 does not always occur, suggesting that additional important triggers beyond host genetics and gut
61 microbes are required (Maloy and Powrie, 2011).

62 The incidence of IBD is increasing in some industrializing countries (Ng et al., 2017) and
63 in immigrant populations that move to industrialized countries (Agrawal et al., 2020). Thus,
64 dietary changes associated with industrialization (*e.g.*, decreased fiber intake, processed foods)
65 may play a role in enhancing disease susceptibility, yet the underlying mechanisms of how diet
66 acts as a disease "trigger" remain unexplored. The physiology of the microbes inhabiting the gut
67 is continuously influenced by diet, especially fiber polysaccharides that elude digestion in the
68 upper gastrointestinal tract and arrive in the ileum and colon providing nutrients for microbes
69 (David et al., 2014; Porter and Martens, 2017). Several studies using murine models fed low
70 fiber or "Westernized" diets have shown alterations in the microbiome that correlate with
71 reduced integrity of the mucosal barrier, including increased activity of mucin-degrading bacteria
72 and reduced mucus thickness (Desai et al., 2016; Earle et al., 2015) and increased mucus
73 permeability (Schroeder et al., 2018).

74 Here, we investigated the specific contributions of dietary fiber and mucin-degrading gut
75 bacteria to the development of spontaneous inflammation in mice lacking the IBD-associated
76 cytokine interleukin-10 (IL-10). In humans, loss of normal IL-10 production or either of its
77 receptor subunits results in early onset IBD in infants and children (Zhu et al., 2017).
78 Conventional *Il10*$^{-/-}$ mice develop spontaneous inflammation that is variable between colonies
79 and worsened by the presence of pathobionts like *Enterococcus faecalis* or *Helicobacter* spp.
80 (Keubler et al., 2015) and housing mice in specific-pathogen-free conditions (Keubler et al.,
81 2015) or deriving as germfree substantially reduces or eliminates inflammation, respectively
82 (Sellon et al., 1998). While it is therefore known that gut microbes are required for disease
83 development in *Il10*$^{-/-}$ mice, the precise mechanisms potentiating disease development in the

presence of commensal bacteria that lack known or potential pathogenic qualities, including the proinflammatory host immune responses, remain unknown.

Our data reveal that a combination of IL-10 loss, a gut microbiota containing mucin-degrading species and a low-fiber diet that increases bacterial mucus erosion are all required to elicit severe disease. At the same time, we observed that the clinically validated dietary therapy exclusive enteral nutrition (EEN) inhibits colitis development, despite lacking dietary fiber, at least in part by promoting production of the bacterial metabolite isobutyrate from soy protein. Our study presents an important step towards unraveling the positive and negative contributions of host genetics, gut microbial physiology and diet on a mechanistic level, and provides first steps towards leveraging the contributions that we can change (diet, microbiome) to reduce the disease burden in people suffering from IBD.

Results

A combination of host genetic susceptibility, low dietary fiber and intestinal bacteria exacerbate colitis

We previously determined that colonization of wild-type germfree mice with a 14-species synthetic microbiota (SM14), which is composed of sequenced and metabolically characterized human gut bacteria, experience erosion of the colonic mucus layer when fed a fiber free (FF) diet. However, these mice do not develop spontaneous inflammation (Desai et al., 2016). To determine if diet- and microbiota-driven mucus erosion—and the corresponding increased proximity of bacteria to host tissue—promotes disease in mice that are genetically susceptible to IBD, we introduced the same SM14 into germfree *Il10*$^{-/-}$ mice. Of note, *Il10*$^{-/-}$ lines have been constructed in several murine strain backgrounds and we chose a C57BL/6J derived line (mouse facility: University of Michigan (UM), USA), which has been reported to be the most resistant to spontaneous disease development (Keubler et al., 2015). We colonized adult 8–10 week old *Il10*$^{-/-}$ mice fed a mouse chow, which we call a fiber rich (FR) diet, for 14 days and switched a subset of the mice to the FF diet after 14 days of colonization, monitoring body weight and microbiota changes for up to 60d. Colonized mice that remained on the FR diet maintained or gained weight and did not experience noticeable morbidity. In contrast, mice switched to the FF diet began losing weight 1–2 weeks after the diet switch and experienced ~75% lethality by 60d (**Fig. 1A**).

114 Histological examination of the intestines of FR and FF fed mice revealed inflammation and
115 epithelial damage that was most severe in the ceca of SM14-colonized FF-fed mice (**Fig. 1B,C**).
116 As expected, similar inflammation did not develop in wild-type mice with the same treatments
117 (**Fig. S1A**–**C**). Cecal measurements of neutrophil-derived lipocalin 2 (Lcn2) provided further
118 quantitative evidence that inflammation was most severe in SM14 colonized *Il10*$^{-/-}$ mice fed FF
119 (**Fig. 1D**). Comparison to colonized FR-fed mice and other treatments that systematically
120 manipulated the individual variables of diet (FR, FF), colonization (SM14 or germfree) and host
121 genotype (wild-type or *Il10*$^{-/-}$) supported the conclusion that severe inflammation only develops
122 in the context of three conditions: IL-10 deficiency, SM14 colonization and low fiber (**Figs.**
123 **1C,D, S1D**).

124 As expected, switching to the FF diet rapidly induced a microbiota shift in favor of
125 decreased fiber-degrading and increased mucin-degrading species in *Il10*$^{-/-}$ mice (**Fig. S1E**). The
126 same trend was observed in wild-type mice fed the FF diet, albeit with significantly increased
127 levels of *E. coli* and *B. thetaiotaomicron* in *Il10*$^{-/-}$ mice (**Fig. S1F,G**). Both of these species have
128 previously been shown to benefit from an inflamed environment (Kitamoto et al., 2020; Morgan
129 et al., 2012), in some cases by sharing iron-scavenging siderophores (Zhu et al., 2020). As
130 expected from studies with wild-type mice fed low fiber (Desai et al., 2016; Earle et al., 2015),
131 feeding the FF diet to *Il10*$^{-/-}$ mice resulted in reduced mucus thickness (**Figs. S1H**–**K**) that likely
132 increases bacterial contact with the host. Moreover, using bacteria-sized florescent beads in an *ex*
133 *vivo* mucus penetrability assay (Schroeder, 2018 #3972), we determined the colonic mucus
134 penetrability. Our results revealed significantly higher mucus penetrability and closer proximity
135 of beads to the host epithelium in FF-fed *Il10*$^{-/-}$ mice compared to their FR-fed counterparts, an
136 effect that was not as pronounced in the wild-type mice with SM14 (**Fig. 1E,F, S1L-M)**. Plating
137 livers and spleens from colonized mice that suffered FF-induced disease on media that support
138 growth of SM14 species did not reveal systemic bacterial dissemination, suggesting that
139 intestinal inflammation, resulting from a damaged mucus barrier and a potentially increased
140 influx of microbial antigens, is the main cause of mortality (not shown).

141 Human disease associated with IL-10 dysfunction presents as early or very early onset
142 IBD in children and infants (Zhu et al., 2017) and germfree mice have underdeveloped immune
143 and mucosal barrier systems (Hooper and Macpherson, 2010) that could contribute to the disease
144 development observed in colonized adult mice. To address these points, we modified our model

145 to allow for microbiota transfer in the neonatal period by colonizing germfree *Il10*$^{-/-}$ adult parents
146 fed the FR diet which allows pups to be exposed to the maternal microbiota beginning at birth.
147 All 14 of the SM species were transmitted, although two of the more fastidious Firmicutes (*F.*
148 *prausnitzii* and *R. intestinalis*) were not transmitted to every pup. As anticipated, the SM14 took
149 on a composition in pre-weaned, milk-fed pups that was similar to that observed in adult FF fed
150 mice (**Fig. S1N**) due to the lack of fiber and the fact that milk oligosaccharides share many
151 linkages in common with mucin *O*-glycans (Marcobal et al., 2011). While there were no signs of
152 disease development during the pre-weaning period, pups weaned to the FF diet began losing
153 weight after ~60 days of age (**Fig. 1G**) and experienced 100% mortality by 105d (**Fig. 1H**). In
154 most experiments, we harvested both FR and FF groups at 100d, in which case mortality among
155 the FF mice was ~85% (**Fig. S1O**). In contrast, all FR-fed mice survived to 100d (**Fig. S1O**) and
156 a separate group of FR-fed mice showed 100% survival when maintained for 150d as did wild-
157 type mice fed either diet (**Fig. 1H**). Weight loss in pups weaned to the FF diet corresponded with
158 increasing fecal Lcn2 that occurred around the same time (60-65d) of declining weight, further
159 suggesting that weight loss is caused by increasing intestinal inflammation (**Fig. 1I**).
160 Interestingly, *Il10*$^{-/-}$ mice raised with a specific pathogen free (SPF) microbiota and fed the FF
161 diet did not lose weight (**Fig. 1G**), showed lower inflammation, measured by Lcn2, at 100d (**Fig.**
162 **1J**), and less histological damage (**Fig. S1P**), revealing that a more complex, murine microbiota
163 does not promote the same level of disease in this model, a point that is addressed in more detail
164 below. Interestingly, SPF mice fed the FF diet *did* exhibit reduced mucus thickness (**Fig. 1K**),
165 implying that it contains mucin-degrading bacteria capable of eroding this layer in a diet-
166 dependent fashion but other factors may offset inflammation development.

167 The FR and FF diets differ substantially in several aspects of their macronutrient
168 composition beyond fiber (**Supplemental Table 1**). To more precisely test the direct impact of
169 fiber, we created modified versions of the FF diet in which 7.5% of the sugar it contains
170 (glucose) was removed and replaced—as close to stoichiometrically as possible—with an
171 equivalent amount of different, food grade purified fibers from oat, wheat or apple. A high sugar
172 diet has been shown to promote inflammation, including in *Il10*$^{-/-}$ mice (Khan et al., 2020). As a
173 control for reducing the sugar concentration, we created a diet that contained the same amount of
174 highly digestible starch, effectively exchanging 7.5% of free glucose for a polymeric form of the
175 same sugar that should still be available to the host via upper GI digestion. Our data reveal that
176 the presence of 7.5% fiber from either of the three sources, but not digestible starch, reduces

177 inflammation measured by Lcn2 (**Fig. 1L**) as well as weight loss and histopathology (**Fig.**
178 **S2A,B**). Even when all of the glucose (44%) was replaced with digestible starch, adult mice
179 colonized with the SM14 developed disease, suggesting that the absence of fiber in this diet is a
180 more prominent contributor to inflammation compared to the high amount of sugar. *B. ovatus*, a
181 proficient degrader of both the pectic and hemicellulosic polysaccharides expected to be present
182 in the supplemental fibers used (Martens et al., 2011), was one of the major responders to the
183 fibers used in these experiments, increasing between 2–3 fold in relative abundance in the
184 community and this increased proliferation occurred at the expense of the mucin degrader *A.*
185 *muciniphila* (**Fig. S2C–G**).

186 To determine if restoring dietary fiber to mice that had already been fed the disease-
187 promoting FF diet is capable of blocking inflammation, we returned colonized adult mice, which
188 ordinarily experience ~75% lethality by 60d, to the FR diet at either 30d or 40d (16 or 26 days
189 after being switched to FF). Both groups of mice that were returned to a high fiber diet exhibited
190 no lethal weight loss and Lcn2 levels and histology at 60d were significantly lower than mice
191 maintained on the FF diet (**Fig. 1M,N**). Interestingly, fecal Lcn2 measurements over time
192 showed that both groups of mice experienced a peak of inflammation after fiber had been
193 restored, which then began declining, indicating that low fiber induces disruption to the host-
194 microbe homeostasis in which inflammation is a lagging effect that can eventually be reset (**Fig.**
195 **1M**).

196

197 **The status of the mucus layer is a critical determinant of inflammation development**

198 To more directly evaluate the disease-promoting role of mucin-degrading bacteria, we
199 colonized adult *Il10*$^{-/-}$ mice with a simpler synthetic microbiota containing only the 10 species
200 (SM10) that have previously been shown not to grow on mucin oligosaccharides (Desai et al.,
201 2016). Mice colonized with a microbiota that lacked the four mucin degraders exhibited 100%
202 survival on the FF diet until 60d post colonization (n=7), lower cecal Lcn2 at 60d (**Fig. 2A**) and
203 reduced histological damage (**Fig. 2B**). Removal of the 4 known mucin-degrading bacteria also
204 corresponded with decreased mucus erosion (**Fig. 2C, S3A**), suggesting that the damage they
205 inflict on mucus integrity is causal to the increased disease activity when they are present.
206 Interestingly, adding back single mucin-degrading bacteria to the SM10 community did not yield
207 the same level of inflammation observed with the full 14-member community, indicating that

208 multiple species may act synergistically to promote more severe disease (**Fig. 2A**). Consistent
209 with the idea that low dietary fiber intake in general promotes the proliferation of mucin-
210 degrading bacteria, the mice colonized with SM10 plus a single mucin degrader all exhibited
211 expansion of that mucin-degrading bacterium either before or after the diet switch compared to
212 SM14 (**Fig. S3B–G**). This is in contrast to mice colonized with the full SM14, which typically
213 show the largest expansion of *A. muciniphila* and *B. caccae* in response to low fiber (**Fig.**
214 **S1E,F**). Despite promoting significantly less Lcn2 production, the presence of either *Bacteroides*
215 *thetaiotaomicron* or *Akkermansia muciniphila* as the sole mucin-degrader produced histological
216 inflammation that was statistically identical to the full SM14 (**Fig. 2B**) and this appeared
217 qualitatively worse with only *A. muciniphila* (**Fig. 2D**) despite the lack of weight loss and lower
218 Lcn2.

219 As a separate test of the protective role for mucus in this colitis model, which could
220 potentially be influenced by the presence of dietary fiber in other ways, we bred *Il10*$^{-/-}$*Muc2*$^{-/-}$
221 double knockout (DKO) germfree mice, colonized them with the SM14 and fed either the FR or
222 FF diets. As expected, these mice lost weight quickly (100% needed to be sacrificed before 30d
223 on FF and before 34d on FR; n=5 and 7, respectively) and showed severe inflammation and
224 mortality regardless of diet (**Fig. 2E-I**). Along with the experiments to replace some or all
225 dietary glucose with highly digestible starch, these results suggest that the high sugar in the FF
226 diet is not the main driver of disease since the low sugar FR diet also promotes inflammation
227 when the mucus layer is genetically eliminated. Interestingly, inflammation in DKO mice
228 developed throughout the lower intestine and was more severe in the colon than in the cecum
229 (**Fig. 2H,I**). This is likely due to the mucus system being thinner and more patchy in the cecum
230 than in the colon (Furter et al., 2019). Thus, when *Il10*$^{-/-}$ mice experience low fiber-induced
231 mucus erosion, the barrier function is likely to fail first in the cecum. In contrast, in DKO mice
232 the uniform elimination of Muc2 appears to promote more widespread inflammation that is
233 worse in the colon.

234

235 **Mucin-degrading bacteria influence the inflammatory immune pathways in a genetically**
236 **susceptible host**

237 Development of spontaneous intestinal inflammation is a complex process involving innate
238 and adaptive immune responses, and the role of Th1/Th17 cells has been characterized in the *Il10*$^{-}$

239 $^{/-}$ colitis model in conventional and SPF settings (Keubler, 2015 #23R). Nevertheless, how specific
240 microbial triggers influence the underlying immune pathways and how these immune responses
241 develop temporally remain unknown. Given our contrasting colitis phenotypes in FF-fed SM14-
242 and SM10-colonized *Il10*$^{-/-}$ mice, our SM model provides important opportunities to tease apart
243 not only the microbial triggers but the regionality, timing and severity of underlying inflammatory
244 immune pathways associated with increased microbial mucin foraging driven by fiber deficiency.
245 We repeated the same experiments described above with a different line of *Il10*$^{-/-}$ mice in the
246 C57BL/6J background (mouse facility: University of Luxembourg (UoL), Luxembourg) and
247 observed a similar weight loss in FF-fed mice colonized with SM14 (**Fig. S3H,I)**, validating our
248 results in a different laboratory setting.

249 Cytokine measurements in cecal tissues revealed expected increases of IBD-associated
250 markers IL-1β, IL-6, IL-17, IL-22, IL-23, TNF-α and IFN-γ in fiber-deprived *Il10*$^{-/-}$ mice that were
251 either colonized with SM14 as adults or colonized at birth from maternal exposure (**Fig. S3J-X)**.
252 In addition, we observed that *Il10*$^{-/-}$ mice colonized maternally from birth with the SM10 lacking
253 mucin degraders recapitulated the reduced disease phenotype observed in adults (**Fig. S3H,I**). In
254 these SM10-colonized mice, fiber deprivation only slightly induced the expression of IL-17, IL-
255 22 and TNF-α that were elevated in SM14-colonized mice (**Fig. S3T-W**). Combined with the
256 region-specific inflammation effects (*i.e.*, cecal vs. colonic inflammation in *Il10*$^{-/-}$ and DKO mice),
257 this observation provided an opportunity to examine the sequential and regional involvement of
258 host immune responses in the development of spontaneous colitis.

259 In SM14-colonized mice that were weaned to the FF diet, inflammation could be detected
260 in the cecum via increased Lcn2 as early as 35 days post weaning (dpw) and this effect was absent
261 in mice colonized from birth with SM10 (**Fig. 3A**). SM14 mice weaned onto the FF diet also
262 exhibited low fecal Lcn2 at 35 dpw, consistent with data shown above and supporting the
263 conclusion that disease develops earlier in the cecum in mice with intact mucus production (**Fig.
264 3A**). An expansion of natural killer (NK) cells was detectable in the cecum and colon of FF-fed
265 mice as soon as 35 dpw (**Fig. 3B, left panel**). Interestingly, this expansion was similar in SM10-
266 and SM14-colonized ceca, but NK cells were lower in the colons of SM10-colonized mice
267 compared to those with SM14 (**Fig. 3B**). This latter observation suggests that the presence of
268 mucin-degrading bacteria is more important to elicit this effect in the colon where the mucus
269 system is thicker and mucus erosion is required to increase contact with bacterial antigens.
270 Interestingly, SM14-colonized wild-type (WT) mice also showed increased NK cells in the colon

271 at 79 dpw compared to FR-fed controls, implying that IL-10 dysfunction is not required to elicit
272 increased NK cell infiltration (**Fig. S4A,B**).

273 While NK cells were more abundant at 35 days and later decreased, T cell recruitment
274 (especially $CD4^+$ T cells) increased over time in both the cecum and colon of colonized *Il10*$^{-/-}$ mice
275 **(Fig. 3C and S5A,B)**. In the ceca of colonized *Il10*$^{-/-}$ mice, fiber deprivation increased both $CD4^+$
276 and $CD8^+$ T cell populations by 35 dpw, with $CD4^+$ T cells increasing further by 79 dpw
277 independently of the diet **(Fig. 3D,E)**. In the ceca of germfree *Il10*$^{-/-}$ mice and SM14-colonized
278 WT mice, $CD8^+$ T cells and $CD4^+$ T cells were also more abundant in FF-fed than in FR-fed mice,
279 suggesting that fiber deprivation induces T cell recruitment through multiple paths and not all of
280 these are regulated by the microbiota and IL-10 **(Fig. 3D,E and Fig. S4B)**.

281 Consistent with previous descriptions of *Il10*$^{-/-}$ colitis, both SM10- and SM14-colonized
282 mice generally exhibited infiltration of Th1 and Th17 cells over time. Especially for Th17 cells,
283 this infiltration was higher in FF-fed mice in both the cecum **(Fig. 3E)** and the colon **(Fig. 3F)**.
284 While Th17 cells reached nearly equivalent levels at 79 dpw in SM10 and SM14-colonized ceca
285 (**Fig. 3E**), overall levels were lower in the SM10-colonized colons compared to SM14.
286 Furthermore, fiber deprivation increased Th1 levels in the SM14-colonized colons, but not in the
287 SM10-colonized ones (**Fig. 3F**), which supports the weight loss observed in FF-fed SM14
288 colonized animals. In line with the readouts mentioned above, this observation supports the idea
289 that the role of mucin-degrading bacteria is far more important in the colon where erosion of mucus
290 facilitates the induction of the anti-microbial Th1 responses. To provide functional support to these
291 immune cell profiles, we compared levels of Th1- and Th17-type cytokine transcripts in ceca and
292 mesenteric lymph nodes using qPCR between 35 and 79 dpw. Fiber deprivation led to increased
293 expression of Th1 (IFN-γ, TNF-α, IL-6, IL-12) and Th17 cytokines (IL-17F, IL-22, IL-23 and
294 TGF-β), as well as the mucin-inducing cytokine IL-13 in SM14-colonized *Il10*$^{-/-}$ mice **(Fig. S3T-**
295 **W and S5C)**. These cytokine responses tended to develop more slowly in SM10-colonized mice
296 compared to those with SM14 (**Fig. S3T-W**). In the colon-draining MLNs where naïve T cells get
297 activated and polarized, the Th17-related cytokines, IL-17F and IL-22, were increased by fiber
298 deprivation in both SM10- and SM14-colonized mice, while the Th1-polarizing cytokines IFN-γ,
299 IL-6 and IL-12 were only increased in SM14-colonized mice, consistent with a regional
300 dependence on mucin-degrading bacteria to develop Th1 responses (**Fig. 3G**).

301 Despite the IL-10 deficiency, $Foxp3^+$ regulatory T cell (Treg) recruitment was also
302 detectable and higher during FF-feeding of SM14 *Il10*$^{-/-}$ mice **(Fig. 3H, S5D)**. This expansion

being independent of IL-10 suggests a mechanism driven by other regulatory mediators such as TGF-β, whose transcript levels increased in SM14-colonized cecal tissues as soon as 35 dpw (**Fig. S3Y**). Regulatory T cells expressing Tbet or RORγt have been proposed as counter-regulators of inflammatory Th1 and Th17 cells, respectively (Barros et al., 2022; Yang et al., 2016). Consistent with this, the abundance of Tbet^{+} Treg cells follow the same trends as inflammatory Th1 cells with higher levels in FF-fed, SM14-colonized mice **(Fig 3H and S5E)**. By contrast, the highly suppressive RORγt^{+} Treg population was reduced at 35 dpw in the colon **(Fig. 3H)** and at 79 dpw in the cecum of FF-fed, SM14-colonized *Il10*$^{-/-}$ mice **(Fig. S5E)**, thus favoring the inflammatory responses. In addition, Gata3^{+} Tregs were increased in fiber-deprived GF ceca **(Fig. S4B)** and colonized colons **(Fig. 3H)**. While their role in the specific regulation of type 2 inflammatory cells is still unclear, they may constitute a reservoir of Tregs required for tissue repair by 79 dpw in colonized colons (Wang et al., 2011; Wohlfert et al., 2011).. Finally, despite the general expansion of Treg, early (35 dpw) loss of the highly suppressive RORγt^{+} subset and the IL-10 deficiency are likely to allow the Th1/Th17 responses to flourish in FF-fed, SM14 mice. Together, these results reveal strong Th1/Th17 immune pathways induced by fiber deprivation, differentially regulated by microbial community members and host genetics, in a time- and intestinal site-specific manner.

Alterations to IgA–microbiota interactions precede inflammation

The identities of SM14 bacteria that serve as potent immune stimulators might be different from those involved in degrading mucus. Since coating with immunoglobulin A (IgA) has been proposed to identify bacteria that are potentially more colitogenic (Palm et al., 2014), we next focused on how low fiber-induced inflammation development alters bacterial IgA coating in our *Il10*$^{-/-}$ model. The IgA response is a common anti-microbial response in the gut and is usually upregulated in colitis in human and mouse models (Gomes-Santos et al., 2012). Mirroring the trend observed for early inflammation (**Fig. 3A**), soluble IgA titers were increased in the cecum but not feces of FF-fed SM14-colonized *Il10*$^{-/-}$ mice at 35 dpw compared to FR **(Fig. 4A)**. However, FF-feeding induced a depletion of IgA-producing plasma cells in both the cecum and colon (**Fig. 4B**). This loss was also observed in FF-fed WT mice, suggesting a diet-driven effect on IgA-producing cell loss rather than a depletion caused by the absence of IL-10. This is in line with a published report showing reduced titers of serum IgA and less IgA^{+} B cells in the small intestine of WT mice fed a zero-fiber diet compared with a high-fiber diet (Tan et al., 2016). In parallel with reduced IgA-producing cells after FF-feeding, the proportion of IgG-producing cells was increased at 35

335 and 79 dpw in both cecum and colon of SM14-colonized *Il10*$^{-/-}$ mice **(Fig. S6A and S6B)**.
336 Consistent with the high production of Th1 cytokines in the presence of mucolytic bacteria, FF-
337 feeding increased the proportion of IgG-producing cells only in SM14- but not in SM10-colonized
338 colons **(Fig. S6**B**)** (Castro-Dopico et al., 2019).

339 We next sought to determine how changes in IgA producing cells are reflected in bacterial
340 IgA coating. Intriguingly, analysis of IgA-coated bacteria revealed the presence of 2 differentially
341 coated populations in FR-fed mice: a large population with low-coating and a smaller population
342 with high coating **(Fig. 4C)**. Consistent with previous studies (Gomes-Santos et al., 2012), the
343 amount of total IgA-coated bacteria (both populations combined) was higher in FF-fed mice than
344 in FR-fed mice by 79 dpw **(Fig. 4D, left)**. However, only the proportion of low-coated bacteria
345 increased in FF-fed mice **(Fig. 4D, right)**, while the highly-coated bacteria were almost absent in
346 fiber-deprived mice, as soon as 21 days of feeding **(Fig. 4D, middle)**. Interestingly, the FF diet-
347 induced increase in total IgA-coating by 79 dpw was not observed in SM10-colonized mice, but
348 was confirmed in SPF *Il10*$^{-/-}$ mice and SM14-colonized WT mice, supporting a mechanism driven
349 by the microbiota rather than the IL-10 deficiency (**Fig. 4E, left**). However, highly-coated bacteria
350 disappeared in SM10-colonized mice as in SM14-colonized mice as soon as 21 dpw (**Fig. 4E,**
351 **middle and S6C**) and low-coated bacteria slightly increased by 79 dpw (**Fig 4E, right**), suggesting
352 a mechanism only partly driven by mucolytic bacteria.

353 Given the altered pattern of IgA production and the fact that IgA coating has been proposed
354 as a marker of bacteria with more colitogenic potential (Palm et al., 2014), we examined the IgA
355 coating of individual SM14 bacterial members. Consistent with an early loss of highly-coated
356 bacteria, changes in IgA-coating indexes in the SM14 community appeared as soon as 21 days of
357 feeding **(Fig. 4F)**. Among the SM14 members, *A. muciniphila*, *D. piger*, *E. coli* and *C. aerofaciens*
358 showed reduced IgA coating index (ICI) values at one or both timepoints in FF-fed *Il10*$^{-/-}$ mice. In
359 wild-type mice, this FF diet-induced reduction in IgA coating was less severe for *A. muciniphila,*
360 but more pronounced for *D. piger*, revealing that IL-10 deficiency affects the IgA-coating profile
361 of commensals in a strain-dependent manner. In contrast, *E. rectale* showed a low ICI in FR-fed
362 mice and this increased with FF-feeding, a condition that corresponds to it being present at low
363 levels, likely due to its inability to compete for mucin-derived nutrients. The causes and effects of
364 variations in IgA coating are still being determined. However, our results clearly demonstrate that
365 different combinations of microbial colonization and diet can alter both the amount and affinity of
366 intestinal IgA, as well as the bacteria that it targets. Along with the data shown above, our results

367 suggest the possibility that the fiber deprivation initiates early disruptions in IgA–microbiota
368 interactions along with a loss of IgA-producing plasma cells allowing *A. muciniphila* and *E. coli*
369 to expand in the absence of high-affinity IgA and contribute to colitis.

370

371 **Different microbiota alter the outcome of diet-induced colitis in *Il10*$^{-/-}$ mice**

372 Because we observed that SPF mice fed the FF diet did not develop inflammation with
373 the same severity as those colonized with SM14 (**Fig. 1G,H**), we performed co-housing
374 experiments in which pups born to SPF- and SM14-colonized mothers were mixed at weaning
375 and exposed to each other's microbiomes. Co-housing SM14-colonized *Il10*$^{-/-}$ pups with SPF
376 mice normalized the weight loss phenotype observed in response to feeding the FF diet (**Fig.**
377 **S4A**). It did not, however, reduce cecal inflammation as measured by both cecal Lcn2 (**Fig. 5A**)
378 or histology (**Fig. 5B**), indicating that weight loss and inflammatory phenotypes can be
379 uncoupled in the presence of different microbes. Mice that were born to SPF mothers showed a
380 more variable response to co-housing with SM14-colonized pups, with only some of these mice
381 developing disease that was often similar in severity to FF-fed, SM14-colonized mice (**Fig.**
382 **5A,B**). Time course analysis of fecal Lcn2 revealed that increased inflammation in co-housed
383 SPF mice occurred after 65 days, a trend that was nearly identical to SM14 mice regardless of
384 their co-housing status (**Fig. 5C**). Although inflammation was variable in co-housed SPF mice
385 there was a positive correlation in the two inflammatory measurements for this group (**Fig. 5D**).

386 The SPF pups are naturally colonized with a natively complex microbiota beginning at
387 birth, whereas the SM14 pups receive a simpler microbiota of known composition. The fact that
388 co-housed SPF pups develop worse inflammation compared to their littermates that are not co-
389 housed suggested that some of the SM14 bacteria are capable of invading the murine SPF
390 microbiota and worsening disease, perhaps synergizing with native murine microbes that
391 perform some of the same metabolic or immunostimulatory functions of other SM14 members.
392 To determine which SM14 species invaded the SPF microbiota and when, we performed 16S
393 rRNA gene sequencing on fecal samples from co-housed mice from both groups over the 100d
394 time course. Our analysis revealed that few of the SM14 bacteria are transferred to SPF mice, a
395 finding that might be expected with human gut bacteria invading a more complex, mouse-
396 adapted microbiota. However, at least 6 members of the SM14 could be detected in co-housed
397 SPF mice, either transiently or at the very end of the time course when inflammation had begun

398 to develop (**Fig. 5E-G, S7B-J**). The most prominent of these invading bacteria was the human
399 commensal *E. coli* strain HS, which appeared in co-housed SPF mice around 22 dpw, prior to the
400 onset of inflammation, and gradually increased, eventually reaching levels >10% in most mice
401 (**Fig. 5E**). Two of the mucin degrading SM14 bacteria (*A. muciniphila* and *Ba. intestinihominis*)
402 showed a similar trend, albeit reaching lower levels and with variability among individual mice
403 (**Fig. 4F,G**). Four other SM14 bacteria (*C. aerofaciens*, *B. uniformis, B. thetaiotaomicron* and *B.*
404 *caccae*) showed transient, small increases around the time (~65d) that inflammation was
405 increasing and these organisms decreased thereafter (**Fig. S7**).

406

407 **Multiple nutrients including protein modify disease development in IBD susceptible mice**

408 A notable characteristic of the FF diet that we used is that its macronutrient composition
409 (**Supplemental Table 1**) resembles some exclusive enteral nutrition (EEN) diets that are used
410 clinically to treat some IBD presentations. EEN diets often contain low or no fiber (Logan et al.,
411 2020) and have proven to be effective at inducing remission of IBD in humans, although the
412 precise mechanism(s) of action is still unknown (Day and Lopez, 2015). Since dysfunction in IL-
413 10 signaling is just one of several host pathways implicated in IBD, it is possible that this
414 particular immune signaling axis is sensitive to lack of fiber, whereas others are not and those are
415 the ones that benefit from EEN. To determine if an EEN diet that lacks fiber promotes
416 inflammation in our gnotobiotic *Il10*$^{-/-}$ model, we weaned SM14 colonized pups onto a
417 commercial EEN diet, which is normally taken as a liquid but in this case was dried, pelleted and
418 sterilized by gamma irradiation (water was provided *ad libitum*). The average weight trajectories
419 of 15 mice (3 separate experiments) supported the conclusion that the low fiber EEN diet
420 promotes some disease development, although not as severe as the FF diet (**Fig. 6A**). Lcn2
421 measurements and histology further revealed a wide amount of variation in the amount of disease
422 present in individual animals, with some mice resembling healthy FR-fed mice, some resembling
423 diseased FF-fed mice and several in between (**Fig. 6B,C**). Despite experiencing less
424 inflammation, the EEN mice still exhibited a reduction in mucus thickness, which we expected
425 given the lack of fiber in the formula used (**Fig. 6D**). Measurements of short- and branched chain
426 fatty acids revealed that mice fed the EEN diet had elevated amounts of the branch-chained fatty
427 acid isobutyrate (**Fig. 6E**) and high isobutyrate in individual animals correlated with those
428 experiencing decreased inflammation (**Fig. 6F**). Isobutyrate is an isomer of the more widely

429 studied, anti-inflammatory short-chain fatty acid butyrate (which was not observed above the
430 limit of detection with the method used) and is derived from L-valine fermentation by certain gut
431 bacteria (Guo et al., 2019). Providing either isobutyrate or butyrate (35 mM) in the drinking
432 water of pups weaned onto the disease-promoting FF diet decreased weight loss (**Fig. 6G**) as
433 well as the amount of inflammation observed (**Fig. 6H,I**), revealing that either of these
434 molecules can offset the diet- and microbiome-induced damage observed in this model.

435 Feeding the EEN diet promoted changes in the composition of the SM14, which most
436 notably included a ~250-fold increase in the levels of *E. rectale* (**Fig. 6J**). While this Firmicute is
437 known to produce butyrate, measurements of culture supernatants from 13 of the SM species in
438 medium supplemented with L-valine plus other peptides did not reveal that *E. rectale* produces
439 isobutyurate under the medium conditions tested. Rather, this metabolite was produced by all of
440 the *Bacteroides, plus M. formtaexigens* (**Fig. 6K**). Because isobutyrate is thought to derived from
441 protein (L-valine) fermentation in the colon, we examined the protein sources in our disease
442 promoting FF diet and the partially protective EEN diet, noting that the former contains
443 exclusively casein and the latter contains a mixture of soy protein and casein (**Table S1**), with
444 soy protein listed first in the ingredients and therefore more abundant. To test the hypothesis that
445 soy protein directly or indirectly fuels microbial production of isobutyrate that, in turn, protects
446 against inflammation, we produced a version of the FF diet (FF-soy) in which casein was
447 replaced with soy protein and all other components remained nearly identical (**Table S1**, notably
448 the soy protein isolate that we used was determined to contain contaminating fiber (7% w/w),
449 which ultimately contributed 1.6% fiber to the FF-soy diet). Interestingly, the modified FF-soy
450 diet resulted in a similarly variable phenotype as the EEN diet, characterized by several animals
451 being protected from disease as determined by weight loss, Lcn2 and histological measurements
452 (**Fig. 6H,I**). FF-soy fed mice contained more cecal isobutyrate than FF-fed mice consuming only
453 casein protein (**Fig. 6L**). As with EEN feeding, the amount of isobutyrate was inversely
454 correlated with inflammation severity, although not as strongly in the FF-soy fed mice as in EEN
455 (**Fig. 6M**). Interestingly, several of the FF-soy fed mice exhibited Lcn2 levels that were as much
456 as 10-fold lower than the healthy FR fed mice (**Fig. 6H**). This latter observation could be due to
457 the residual fiber (1.6%) in the FF-soy diet synergizing with the protective effects of isobutyrate,
458 even though less isobutyrate is produced in from feeding the FF-soy diet compared to EEN. If
459 this hypothesis can be supported with future work, it raises interesting possibilities to leverage
460 multiple beneficial pathways (fiber fermentation to offset mucus erosion, isobutyrate production

through select bacteria and soy protein feeding) to improve, optimize and perhaps eventually personalize dietary treatments like EEN.

Discussion

The pathophysiology of IBD is complex and variable, in part because of the large number of different genetic contributions that combine with diverse environmental, microbial and dietary triggers that are known or hypothesized to influence its development. The diet-driven inflammation model that was developed and investigated in this study provides both a case study, in which potential contributing factors to IBD can be explored at mechanistic levels, and represents a more general experimental paradigm in which host genetic, immunological, microbiota and dietary factors can be systematically manipulated to examine their effects on disease progression. As examples of spontaneous, genetically-driven intestinal inflammation models continue to be identified and developed (Caruso et al., 2019; Pizarro et al., 2011; Taurog et al., 1999), the ability to work with these murine models in gnotobiotic conditions and with defined diets holds the potential to uncover foundational principles about this complex disease.

The first principle that emerges from the studies reported here is that dietary fiber consumption has the capacity to influence inflammation development. It has been well appreciated that depolymerization of dietary fibers by gut bacteria and fermentation of the resulting sugars leads to beneficial end-products like SCFAs. Metabolism of SCFAs by epithelial and local immune cells strengthens the gut epithelial barrier and promotes immune regulation, both contributing to increased barriers in the lower GI (Smith et al., 2013). Secreted mucus is another important component of the intestinal barrier in the lower GI, in this case being subject to erosion by mucus-degrading bacteria that exhibit increased activity in the absence of dietary fiber (Desai et al., 2016; Earle et al., 2015; Sonnenburg et al., 2005). Defects in mucus glycosylation and status have been associated with IBD in both animals and humans; however, causal connections to increased microbial access through the mucus barrier have been slower to emerge. Perhaps the strongest evidence for causal relationship comes from studying the responses of mice lacking normal mucus glycosylation. As an example, mice lacking core 1 galactosyltranferase, which is required to build core 1 and core 2 *O*-glycan structures, develop spontaneous inflammation (Fu et al., 2011) and this mutation mimics loss of the core 1 synthase molecular chaperone (*cosmc*) an x-linked gene associated with human IBD (Kudelka et al.,

492 2016). Loss of core 3 synthase or double mutants lacking core 1/core 3 are also more susceptible
493 to induced or spontaneous inflammation, suggesting that genetic reductions in mucus
494 glycosylation may increase the rate at which bacteria can erode this barrier through nutrient
495 foraging (An et al., 2007; Bergstrom et al., 2017). Colonic crypts are also protected by mucus-
496 secreted sentinel goblet cells (senGCs), which can be triggered to secrete mucus in response to
497 high levels of bacterial Toll-like receptor ligands in the crypt region (Birchenough et al., 2016).
498 This phenomenon presumably exists to defend the local crypt environment from close microbial
499 encroachment and the observation that samples from IBD patients with active inflammation have
500 reduced numbers of crypts with senGCs suggest that this "tunable" aspect of the mucus barrier
501 can eventually be overwhelmed by frequent bacterial contact (van der Post et al., 2019). Finally,
502 secretion of mucus is tied to sensing of bacterial products like SCFAs (Shimotoyodome et al.,
503 2000), suggesting that there is a complex interplay between the bacteria present to forage on
504 mucus and multiple aspects of dietary fiber (SCFA production from fiber and mucus erosion in
505 its absence). In the future, it will be important to determine how individual bacteria, and
506 individual bacterial communities, vary in their aggressiveness towards degrading mucin, which
507 may be important for the severity of disease that occurs when fiber is absent or diminished from
508 the diet for prolonged periods.

509 Characterization of the immune pathways in SM14-colonized *Il10*$^{-/-}$ mice confirmed the
510 Th1/Th17 mixed profile as previously described in SPF mice (Boyapati et al., 2015), and both
511 pathways worsened under fiber deprivation. The Th1 response is the classical pro-inflammatory
512 pathway leading to tissue damage due to cytotoxicity and oxidative stress, and thus severe
513 pathology in chronic inflammatory settings. By contrast, the pathogenic activity of Th17 cells in
514 colitis is more controversial, as they produce both IL-17A and IL-22, which have showed
515 opposite properties in the *Il10*$^{-/-}$ mouse model (Gunasekera et al., 2020; Tachibana et al., 2020).
516 Interestingly, in our model, we were able to show that removing the mucin-degrading bacteria
517 prevented completely and partially the FF-diet-increased Th1 and Th17 responses, respectively,
518 suggesting limited Th1-mediated tissue damage but conserved Th17-driven anti-microbial and
519 tissue repair responses. In addition, we report the recruitment of NK cells early in the
520 pathogenesis (35dpw), before the acute infiltration of T cells, and this recruitment is worsened
521 under fiber deprivation. Despite their cytotoxic properties and potent pro-inflammatory abilities,
522 NK cells have been poorly described in the context of colitis. Unexpectedly, they were reported
523 to reduce disease in the T cell transfer model of colitis by preventing T cell effector functions

524 (Fort et al., 1998). However, we cannot exclude that perforin and other cytotoxic molecules have
525 direct tissue damage effects when NK cells are overrepresented as under fiber deprivation.

526 IgA–gut microbiota interactions are known to change based on the microbial composition
527 or diet (Huus et al., 2020; Huus et al., 2021; Kau et al., 2015; Nakajima et al., 2018), and have
528 been implicated in the development of IBD (Palm et al., 2014). Our data suggest that the host
529 immune responses directly affect the IgA-coating of bacteria. The SM14-colonized *Il10*$^{-/-}$ mice
530 have more cecal and fecal IgA, more IgA-coating; and, both are increased under fiber
531 deprivation and are regulated by the presence of mucin-degrading bacteria. Similarly, the high-
532 coated fraction present under the FR diet is lost under fiber deprivation, which is in line with the
533 loss of IgA-producing plasma cells in the colonic lamina propria. Our study suggests a possible
534 association of this high coated fraction to plasma cell-derived high-affinity and specific IgA,
535 although further work is needed to confirm that the loss of this fraction is due to the loss of
536 specific IgA production. In line with our data, previous studies have reported altered interactions
537 between bacteria and IgA, due to direct dietary selective pressure on bacterial strains with altered
538 glycan profiles, thus altering non-specific glycan interactions between the two parts (Huus et al.,
539 2020). Interestingly, fiber deprivation increases the relative abundance of *A. muciniphila* and
540 decreases its IgA-coating, suggesting that the diet selects for *A. muciniphila* cells (or possibly
541 substrains) that are able to escape the Ig trapping and further induce immune responses. In
542 support of this hypothesis, *A. muciniphila* monocolonization was reported to induce
543 inflammation in *Il10*$^{-/-}$ mice, and more particularly the expression of Th1-associated cytokines
544 (IFNg, IL-12, IL-1b, TNFa, IL-6) but not Th17-associated cytokines (IL-22 and TGFb),
545 compared to *Bacteroides acidifaciens*-monocolonized mice (Seregin et al., 2017).

546 The discovery that the EEN diet tested here exerts partial protection against inflammation
547 was fortuitous. Our hypothesis that any diet lacking microbiota accessible fiber would exert
548 detrimental effects by increasing the activity of mucus-degrading bacteria was not fully
549 supported when we fed mice the EEN diet. However, this result may be unsurprising given the
550 complexity of diet-microbiome-host interactions that occur in the gut. The EEN diet used clearly
551 holds the potential to elicit mucus layer erosion, as well as inflammation in some animals, which
552 we attribute to its lack of fiber along with other potential contributing factors. However, the
553 finding that the protein source deployed in a therapeutic diet has the capacity to modify its effect
554 through supplementation of an orthogonal microbial metabolic pathway provides new insight.

555 The mechanism by which soy protein provides increased resources, presumably via L-valine or
556 peptides containing this amino acid, to isobutyrate-producing bacteria remains to be resolved.
557 Soy protein isolate is known to harbor protease inhibitors that are not fully denatured by heating
558 or extraction (Kakade et al., 1976). Protease inhibitors could retard digestion in the upper GI,
559 yielding increased protein for colonic bacteria to ferment. If this is true, the bacteria that
560 participate in this response would presumably need to possess mechanisms to overcome protease
561 inhibitors. While a shift towards high protein fermentation is often regarded as deleterious due to
562 increased production of metabolites like hydrogen sulfide, it is possible that gaining a deeper
563 understanding of the microbial mechanism(s) at play in our model will illuminate a path to
564 leverage cheap and abundant soy protein to treat inflammation while minimizing deleterious
565 effects. Such a path might include treating or digesting crude soy protein isolate to enrich for the
566 components that promote isobutyrate, while minimizing bulk protein fermentation in the colon. It
567 remains possible—perhaps likely—that isobutyrate production from soy protein is not the major
568 mechanism of action of EEN treatment in humans. Still, the discovery of a new dietary route to
569 influence the production of anti-inflammatory metabolites through the gut microbiota presents an
570 additional path to help improve gut health and could be optimized in future EEN formulations or
571 other supplements. Towards this points, identifying the critical bacteria in our SM14 and their
572 corresponding pathways for soy protein assimilation and isobutyrate production will be essential
573 and could illuminate why ~15% of patients given EEN do not respond (Adamji and Day, 2019),
574 perhaps because they are missing these bacteria/pathways.

575 Many questions remain regarding the development of the multifactorial diseases
576 encompassed under IBD. While host genetic susceptibility is a mostly permanent trait that it
577 difficult to repair, an exception being stem cell transplant in children lacking IL-10 signaling
578 (Kakade et al., 1976), the microbiome and especially diet are factors that can potentially be
579 manipulated to delay or reverse disease. Comparison of SPF and SM14-colonized *Il10*$^{-/-}$ mice,
580 with and without co-housing, highlights that the particular microbiota present have the capacity
581 to modify disease, possibly through variations in microbial diversity or contributions of multiple
582 counter balancing pathways (*e.g.*, mucin degradation, isobutyrate production, other metabolites
583 like SCFA). Our co-housing results suggest that more complex relationships are also possible,
584 such as effects of sequential or co-colonization by different bacteria. Ever since the discovery
585 that rearing *Il10*$^{-/-}$ mice under germfree conditions abrogates inflammation (Sellon et al., 1998),
586 there has been great interest in finding specific bacteria or bacterial combinations that elicit

587 inflammation when added back to these animals. This search has yielded significant insight into
588 the contributions of bacteria with known pathogenic qualities, such as *Helicobacter* spp.,
589 *Enterococcus faecalis* and adherent invasive *E. coli* (Keubler et al., 2015). However, roles for
590 specific commensal bacteria have also been established using gnotobiotic mice (Packey and
591 Sartor, 2009), albeit without a clear understanding of the mechanism(s) involved. Based on the
592 data presented here, we propose a model that is focused more on the influence of positive and
593 negative bacterial metabolic pathways and not on specific bacterial taxa. The rationale for this
594 view is that metabolic pathways like mucin degradation can be present in diverse bacteria and
595 these organisms may fulfill similar roles in eroding mucus. In contrast, strains of the same
596 species can vary in key metabolic capabilities, including mucus degradation, which is known to
597 vary substantially among strains some of *Bacteroides* (Pudlo et al., 2022) and likely other
598 groups. If one considers the effects of the microbiome on IBD development to be an cumulative
599 series of positive and negative stimuli caused by the particular behaviors and metabolites
600 exhibited by the microbes present, it should be possible to optimize beneficial processes (*e.g.*,
601 butyrate, isobutyrate) while reducing detrimental events like mucus erosion. While some of these
602 levers can be manipulated through diet, a promising path for intervention may eventually include
603 adding or replacing specific bacterial taxa within a person's individual microbiota with more
604 optimal strains or perhaps even those that are engineered to increase beneficial metabolites.

605

606 **Materials and Methods**

607 **Animal models, colonization and sample processing**

608 Animal experiments at the University of Michigan followed protocols approved by the
609 University of Michigan and the University Committee for the Use and Care of Animals. Germ-
610 free B6.129P2-Il10tm1Cgn/JZtm mice (Institut für Versuchstierkunde und Zentrales
611 Tierlaboratorium, Hannover, Germany) and wild-type C57BL/6J (University of Bern,
612 Switzerland) were bred at the animal facility of the University of Luxembourg and underwent
613 protocols approved by the Animal Experimentation Ethics Committee of the University of
614 Luxembourg and the Ministre de l'Agriculture, de la Viticulture et du Developpement rural du
615 Grand-Duché du Luxembourg (LUPA 2020/20). Germfree males and females were colonized at
616 7-9 weeks of age and none of these mice was involved in any previous experiments/treatments.
617 Mice were either housed alone or in groups of appropriate gender, litter, and dietary experiments.

618 Food and autoclaved distilled water were provided ad libitum. The Muc2$^{-/-}$ were also crossed to
619 C57BL/6J background were obtained from Leonard Augenlicht (Einstein University). For the
620 generation of IL-10$^{-/-}$ Muc2$^{-/-}$ double knockout (DKO), the single KO mice were crossed to obtain
621 double heterozygous mice until generation of IL-10$^{-/-}$ Muc2$^{+/-}$. Full double KO mice developed
622 spontaneous prolapse in germ-free condition during prolonged breeding periods, thus, the IL-10$^{-/-}$
623 Muc2$^{+/-}$ mice were used to generate the double KO mice used for all experiments. Genotyping was
624 performed by extracting DNA from ear punches (Transnetyx). Mice were gavaged with the
625 synthetic microbiota at 6-8 weeks and proceeded to diet change as previously described. The
626 synthetic microbiota bacteria were grown in their respective medium or a modified YCFA medium
627 (Steimle et al., 2021) prior to community assembly for gavages. The bacteria were cultivated under
628 anaerobic atmosphere maintained with a gas mixture (85% N_2, 10% H_2, 5% CO_2) to an optical
629 density (absorbance 600nm) ranging from 0.5 to 1.0. The communities were assembled by mixing
630 equal volumes of each specific bacterium and aliquoted into sealed screw cap tubes with its own
631 headspace. Each mouse was gavaged with 0.2 mL of its specific community, depending on the
632 experiment, with freshly prepared inocula for two-three consecutive days. Animals were
633 euthanized using CO_2 asphyxiation for 5 minutes followed by cervical dislocation. The
634 gastrointestinal tracts were retrieved quickly, to prevent autolysis, and the sections separated.
635 Cecal and colon contents of each animal were flash frozen in liquid nitrogen and kept at -80°C
636 until further use.

637 The colons were sectioned from the colon-cecum junction to the anus, and immediately
638 fixed in freshly made Carnoy's fixative (methanol:chloroform:glacial acetic acid, 60:30:10 v/v).
639 The distal part of the small intestine was fixed in freshly made Carnoy's fixative together with the
640 half blunt end of the cecum. Fixed tissues were kept in Carnoy's fixative for three hours and
641 exchanged for fresh fixative for another 24 hours. The tissues were then washed in 100% methanol
642 and kept until placed in cassettes for histology preparation. Cecal contents of each animal were
643 flash frozen in liquid nitrogen and kept at -80°C until further use. The remaining empty half of the
644 cecum were flash frozen in liquid nitrogen and kept at -80°C until further use.

645

646 **DNA extraction**

647 DNA from fecal and cecal samples were isolated using a bead-beating phenol:chloroform
648 extraction method followed by DNeasy Blood & Tissue Kit (QIAGEN, USA). In short, samples

649 were weighed between 10-50mg and combined with acid-washed glass beads (212-300mm;
650 Sigma-Aldrich, USA), 500uL Buffer A (200 mM NaCl, 200 mM Tris, 20 mM EDTA, 210 uL SDS
651 (20% w/v, filter-sterelized), and 500 uL phenol:chloroform (Thermo Fisher Scientific, USA). The
652 samples were disrupted using a Mini-Beadbeater-16 (Biospec Products, USA) for 3 minutes at
653 room temperature and centrifuged (10,000 rpm, 4°C, 3 minutes). The aqueous phase was recovered
654 and mixed with an equal volume of phenol:chloroform by gentle inversion and centrifuged (10,000
655 rpm, 4°C, 3 minutes). The remaining aqueous phase was recovered and mixed with 500 µL of
656 chloroform, mixed by gentle inversion, and centrifuged (10,000 rpm, 4°C, 3 minutes). Recovered
657 aqueous phase was mixed with 1 volume of isopropanol and 1/10 volume of 3M sodium acetate,
658 and stored at -80°C for 20 minutes for DNA precipitation. Samples were centrifuged (15000 rpm,
659 4°C, 20 minutes), supernatant discarded, washed with 70% ethanol, air-dried, and resuspended in
660 nuclease-free water. The sample DNA extracts were further purified with DNeasy Blood & Tissue
661 kit, following manufacturer protocol (QIAGEN).

662

663 **RNA extraction, reverse transcription and qPCR**

664 Freshly retrieved ileal, cecal and distal colon tissues were transferred into RNAlater™
665 (QIAGEN) and kept at 4°C up to a week. Then, RNAlater™ was removed and tissues were stored
666 at -80°C until further use. Frozen tissues were transferred into 1 mL of TRIzol reagent
667 (Invitrogen™), homogeneized with a 5 mm metal bead on a bead beater for 8 min at 30Hz and
668 centrifuged for 3 min at 13000 rpm, 4°C. The supernatant was recovered, mixed thoroughly with
669 200 µl of chloroform and incubated at room temperature for 2-3 min before a centrifigation for 15
670 min at 13000 rpm, 4°C. The aqueous phase was recovered, mixed again with an equal amount of
671 chloroform and centrifuged for 15 min at 13000 rpm, 4°C. The aqueous phase was recovered,
672 mixed by inversion with 500 µl of isopropanol, incubated for 10 min at room temperature, and
673 centrifuged for 10 min at 13000 rpm, 4°C. The pellet was washed with 1 ml Ethanol 70% and
674 centrifuged for 5 min at 10000 rpm. The supernatant was discarded and the pellet dried for 5-10
675 min at 37°C, resuspended with 50 µl nuclease-free water and incubated for 15 min at 56°C. Finally,
676 samples were treated with DNase following the Thermo Scientific DNase1, RNase-free Protocol,
677 and RNA were purified with the RNeasy Mini kit (QIAGEN) according to manufacturer
678 instructions. Final RNA concentrations were quantified by Nanodrop.

679

680 **Lipocalin 2 (Lcn2) measurements in cecal and fecal contents**

681 Frozen cecal and fecal samples were used to quantify the presence of lipocalin-2 protein
682 (LCN2) by enzyme linked immunosorbent assay (ELISA). Samples previously frozen (cecal, -
683 80°C, and fecal, -20°C) were weighed in new tubes between 5-5 mg. Samples were kept over dry
684 ice during the weighing. Samples were resuspended in 1 mL PBS (pH 7.4), vortexed for 30s, and
685 kept at 4°C overnight to homogenize. Samples were then extensively vortexed to a homogeneous
686 solution. To measure the LCN-2 levels, a DuoSet mouse lipocalin-2/NGAL ELISA kit (R&D
687 Biosystems, USA) was employed using several dilutions of sample homogeneous solution.
688 Quantification was done following manufacturer protocol.

689

690 **Soluble IgA measurements in cecal and fecal contents**

691 To measure soluble IgA levels, Nunc® MaxiSorp™ 384 well plates (Sigma-Aldrich) were
692 coated overnight with 10 ng/well rabbit anti-mouse IgA (Novus Biologicals, Bio-Techne NB7506)
693 in 20 µl/well of carbonate-bicarbonate buffer (Sigma, Ref.: C3041). After four washes with
694 Washing Buffer (1% Tween-20, 154mM Sodium Chloride and 10mM Trisma-base), 75µl of
695 Blocking Buffer (15 mM Trizma-Acetate, 136 mM Sodium Chloride, 2 mM Potassium Chloride
696 and 1% (w/v) BSA (Bovine Serum Albumin)). After 2h at room temperature, wells were washed
697 again. Sample homogeneous solution and standards (mouse IgA Isotype Control UNLB, Southern
698 Biotech, Imtec Diagnostics, Ref: 0106-01) were diluted in Dilution Buffer (15 mM Trizma-
699 Acetate, 136 mM Sodium Chloride, 2 mM Potassium Chloride, 0.1% (w/v) Tween-20, and 1%
700 BSA) and incubated into the plate at 20 µl/well, room temperature for 90 min. After washing, 20
701 µl/well of a Phosphatase Alkaline-conjugated goat anti-mouse IgA (Southern Biotech, Imtec
702 diagnostics, Ref: 1040-04), diluted 1/1000 in Dilution Buffer, was added and incubated at room
703 temperature for 90 min. After a final wash, 40 µl/well of substrate (1 phosphate tablet (Sigma, ref
704 S0642-200 TAB) dissolved in 10 mL Substrate Buffer (1 mM 2-Amino-2-methyle-1-propanole,
705 0.1 mM MgCl2.6H2O)) was added. The plate was incubated at 37°C for 60 min before the
706 absorbance was measured at 405 nm using an ELISA plate reader (SpectraMax Plus 384
707 Microplate Reader from Molecular Devices; Software: SoftMax Pro 7 Software, Molecular
708 Devices). The IgA concentration was determined for each sample using the formulated standard
709 curve.

710 **Short- and branched-chain fatty acid quantification**

711 Flash frozen cecal content samples stored at -80°C were used to quantify short-chain fatty
712 acids (SCFAs) and branched-chain fatty acids (BCFAs). Firstly, the samples were thawed in ice
713 and weighed (50-100 mg). Samples were resuspended in 500 µL of Milli-Q water, thoroughly
714 vortexed to homogeneity and centrifuged (15000 rpm, 4°C, 20 minutes). The supernatant was then
715 filtered through a 0.22 µm (Millex-gv 4mmSLGV004SL) and pipetted into HPLC vials. Samples
716 were run on a Shimadzu HPLC with an Agilent HP-87X column, to separate the compounds, with
717 a 0.01N H2SO4, flow rate of 0.6mL/min, and column temperature of 50°C. A UV detector set to
718 a wavelength of 214 nm and a RID were used to detect compounds. A standard curve of known
719 concentrations was used to quantify the different compounds (lactate, acetate, succinate,
720 propionate, isobutyrate, butyrate, and isovalerate).

721

722 **Lamina propria cell extraction and flow cytometry analysis**

723 Cecal and colonic lamina propria cells were extracted using the Lamina Propria
724 Dissociation Kit and gentleMACS Dissociators (Miltenyi Biotec, Germany) according to the
725 manufacturers instruction. After digestion, cells were resuspended in PB buffer (PBS, pH 7.2, 0.5
726 % BSA) and counted. For analysis of T cells and ILCs with the expression of transcription factors,
727 the FOXP3/Transcription Factor Staining Buffer kit (eBioscences – 00-5523-00) was used along
728 with the following anti-mouse antibodies: BV605-conjugated anti-CD4 (Biolegend, RM4-5;
729 1/700), BV650-conjugated anti-B220 (BD Biosciences, RA3-6B2; 1/88), BV711-conjugated anti-
730 CD3 (Biolegend, 17A2; 1/88), BV780-conjugated anti-CD45 (BD Biosciences, 30-F11; 1/88),
731 FITC-conjugated anti-CD335/NKp46 (Biolegend, 29A1.4; 1/100), PE-Cy5-conjugated anti-CD8
732 (Biolegend, 53-6.7; 1/700), eF450-conjugated anti-FoxP3 (eBiosciences, FJK-16s; 1/200), PE-
733 conjugated anti-GATA3 (Biolegend, 16E10A23; 1/44), PE-eF610-conjugated anti-EOMES
734 (eBiosciences, Dan11mag; 1/100), PE-Cy7 -conjugated anti-Tbet (Biolegend, 4B10; 1/44), APC-
735 conjugated anti-RORgt (eBiosciences, AFKJS-9; 1/22). For B cells analysis and immunoglobulin
736 expression, the BD Cytofix/Cytoperm^{TM} Fixation/Permeabilization Solution Kit (BD Biosciences
737 – 554714) was used along with the following anti-mouse antibodies: eF450-conjugated anti-
738 B220/CD45R (eBiosciences, RA3-6B2; 1/700), eF506-conjugated anti-CD19 (eBiosciences, 1D3;
739 1/88), BV711-conjugated anti-CD3 (Biolegend, 17A2; 1/88), BV780-conjugated anti-CD45 (BD
740 Biosciences, 30-F11; 1/88), APC-conjugated anti-CD138 (Biolegend, 281-2; 1/100), FITC-

741 conjugated anti-IgA (eBiosciences, mA-6E1; 1/700), PerCP-Cy5.5-conjugated anti-IgD
742 (Biolegend, 11-26c.2a; 1/200), PE-conjugated anti-IgE (Biolegend, RME-1; 1/44), PE-Cy5-
743 conjugated anti-IgM (BD Biosciences, R6-60.2; 1/100), PE-Cy7 -conjugated anti-IgG (Biolegend,
744 Poly4053; 1/44). Breifly, 1.5 million cells were washed twice with PBS prior to 15 min of staining
745 with the Zombie NIR™ Fixable Viability dye (BioLegend – 423105), followed by 2 washes with
746 FACS Buffer (PBS, 5% fetal bovine serum) and fixation according to manufacturer instructions.
747 Cells were then incubated at 4°C for 15 min with Fc Block (Rat anti-mouse CD16 and CD32; BD
748 Pharmingen – Cat.553141) and 30 min with the antibody mixes. Both Fc Block and antibodies
749 were diluted in the permeabilization buffer provided with the fixation kits. Finally, cells were
750 washed twice in their respective permeabilization buffer and resuspended in FACS Buffer for
751 acquisition on a NovoCyte Quanteon Flow Cytometer System (Agilent). The data were then
752 analyzed on FlowJo.

753

754 **Analysis of IgA-coating of bacteria and sorting**

755 Frozen fecal samples were homogeneized in 1 ml ice-cold PBS and centrifuged for 3 min
756 at 100g, 4°C. Supernatant was filtered through a 70 µm straining sieve and centrifuged for 5 min
757 at 10,000g, 4 °C. The pellet was resupended in 1 ml ice-cold PBS, the OD_{600} detected on a
758 Nanodrop and the amount of bacteria computed as follow: 2 OD_{600} = 10^9 bacteria. Bacteria were
759 pelleted again for 5 min at 10,000g, 4 °C, and resuspended in 500 µl of staining buffer (PBS, 5%
760 goat serum). After 20 min of incubation on ice, $1x10^9$ bacteria were washed with 1 ml ice-cold
761 PBS and stained for 30 min at 4°C with 4 µg of FITC-conjugated anti-mouse IgA antibody
762 (Southern Biotech) in 100 µl of staining buffer. Cells were then washed once and resupended in 1
763 ml PBS, and 100 µl of bacteria was pelleted and frozen until further analysis. Remaining bacteria
764 where centrifuged and resuspended in 90 µl of staining buffer and 10 µL of anti-FITC MicroBeads.
765 After 15 minutes of incubation at 4°C, bacteria were washed, resuspended in 500 µl of staining
766 buffer and applied onto a LS column for sorting of IgA^+ and IgA^- fractions with a QuadroMACS™
767 Separator (Miltenyi Biotec). IgA-coated and IgA-uncoated fractions were centrifuged and dry
768 pellets were stored at -80°C until further analysis. For analysis of IgA coating of bacteria, frozen
769 pellets were defrost on ice and washed with 1 ml of staining buffer. Since all samples were not
770 sorted at the same time, bacteria were stained again for 30 min with 0.5 µg of FITC-conjugated
771 anti-mouse IgA antibody (Southern Biotech) in 100 µl of staining buffer to refresh and harmonize

772 the staining between batches. After a washing step, DNA was stained for 20 minutes with diluted
773 1:4000 in 200 µl of DNA staining solution (0.1 M HEPES, 0.9 % NaCl, pH 7.2). Finally, bacteria
774 were washed twice with PBS, fixed for 20 min in 4% PFA, washed again and analyzed on a
775 NovoCyte Quanteon Flow Cytometer System (Agilent). Data were then analyzed on FlowJo. For
776 analysis of IgA affinity, bacteria were treated with 200 µl of PBS containing 3M NaSCN for 15
777 min at 4°C, 800rpm, prior to blocking and staining with FITC-conjugated anti-mouse IgA antibody
778 as mentioned above.

779

780 **Mucus measurements**

781 Slides were deparaffinized by submerging in xylene (Sigma-Aldrich, USA) for five
782 minutes, followed by another xylene incubation for five minutes. Afterward, the slides were
783 dehydrated twice in 100% ethanol for 5 minutes. The slides were then quickly washed in Milli-Q
784 water and antigens were retrieved by submerging in antigen retrieving solution (10 mM sodium
785 citrate, pH 6.0). The submerged sections were heated to 90°C for 10 minutes and cooldown in
786 room temperature for 20 minutes. Slides were quickly dipped three times in Milli-Q water and
787 blotted to remove excess liquid. To better hold liquid, a PAP pen was used to draw around the
788 tissue area for the subsequent steps. The sections were blocked by covering the tissue in blocking
789 buffer (1:10 goat serum (Sigma, USA) in Tris-buffered Saline (TBS; 500 mM NaCl, 50 mM Tris,
790 pH 7.4)) and incubated for an hour at room temperature. For the primary antibody staining, the
791 tissue was covered with a 1:200 dilution of Mucin 2 antibody (H-300) (Santa Cruz Biotechnology,
792 USA) in blocking buffer and incubated for two hours at room temperature. Following the
793 incubation, the slides were rinsed three times in TBS, for five minutes each. The secondary
794 antibody staining was performed by covering the tissue with a 1:200 dilution of Alexa Fluor 488
795 conjugated goat anti-rabbit IgG antibody (Thermo Fisher Scientific, USA) in blocking buffer for
796 one hour at room temperature in dark. The tissue sections were washed twice in TBS for 5 minutes,
797 gently blotted, and covered with ProLong Gold Antifade reagent with DAPI (Invitrogen, USA),
798 covered with cover slips and sealed with nail polish. The slides were kept at room temperature for
799 24 hours in dark, then kept in 4°C until imaging. The mucus layer in the sections were visualized
800 using a Zeiss Apotome by taking pictures across fecal pellets and stitching the images together to
801 compose a single image. Mucus layer measurements were performed by using BacSpace as
802 described by Earle et al.

803 **Mucus penetrability assay**

804 Penetrability of the colonic mucus was assessed as described by Gustafsson et al
805 (Gustafsson et al., 2012). Briefly, colons were flushed with ice-cold oxygenated KREBS Buffer
806 (116 mM NaCl, 1.3 mM $CaCl_2$, 3.6 mM KCl, 1.4 mM KH_2PO_4, 23 mM $NaHCO_3$, and 1.2 $MgSO_4$
807 – Carl Roth) and opened along the mesenteric axis. The longitudinal muscle layer was removed
808 by blunt dissection and the distal mucosa was inserted in a perfusion chamber. The basolateral
809 chamber was filled with 0.6 µg/ml SYTO9 (Fisher Scientific - 10237582) in oxygenated KREBS
810 Glucose Buffer (KREBS Buffer containing 10mM Glucose, 5.7 mM sodium pyruvate and 5.1 mM
811 sodium-l-glutamate), and the apical chamber was filled with oxygenated KREBS Mannitol Buffer
812 (KREBS Buffer, containing 10mM Mannitol, 5.7 mM sodium pyruvate and 5.1 mM sodium-l-
813 glutamate). After 10 min incubation in the dark at room temperature, FluoSphere™ carboxylate
814 beads (1µm, red 580/605 – Invitrogen – F882) were applied on top and let to sediment on the tissue
815 for 5 min in the dark at room temperature. The apical chamber was then gently washed several
816 times to remove excess of beads. The chamber was incubated for 10 min in the dark before being
817 visualized with a microscope. For each tissue, 4-7 confocal images were taken in XY stacks from
818 the epithelium at the bottom to the beads on top, with 5 µm-intervals between sections. Images
819 were then analyzed with Imaris software, and the penetrability was computed by comparing the
820 distance between the outer border of the beads and the epithelium with the distance between the
821 most inner beads and the epithelium.

822

823 **16s rDNA community analysis**

824 PCR and library preparation were performed by the University of Michigan Microbiome
825 Core lab as described by Kozich et al. (Kozich et al., 2013). The V4 region of the 16s rRNA
826 gene was amplified using the dual-index primers described by Kozich et al, 2013. The
827 normalized and amplicon size evaluated samples were sequenced using an Illumina MiSeq. The
828 raw sequences were analyzed using mothur v1.42.3 (Schloss et al., 2009) with the included
829 controls: PBS control during the sequencing and ZymoBIOMICS Microbial Community DNA
830 Standard (cat# D6306) for error analysis. Sequences were aligned to the reference Silva database
831 version 132 for contamination analysis and SPF experiments. Moreover, gnotobiotic mice
832 sequences were also aligned to a custom reference database containing the 16s v4 region from

833 each of the 14 bacteria members. The R package "vegan" was used to calculate the principal
834 component analysis from the Bray-Curtis dissimilarity index.

835

836 **Acknowledgements**

837 We thank the University of Michigan Germfree Core and Microbiome Core for expert
838 technical assistance. We are extremely grateful for support from the Kenneth Rainin Foundation
839 (Innovator Award to ECM) and the US National Institutes of Health (DK118024, DK125445 to
840 ECM). We thank the Luxembourg National Research Fund (FNR) for CORE grants to M.S.D.
841 (C15/BM/10318186 and C18/BM/12585940); E.T.G. was supported by FNR PRIDE
842 (17/11823097) and the Fondation du Pélican de Mie et Pierre Hippert-Faber, under the aegis of
843 the Fondation de Luxembourg; M.B. was supported by a European Commission Horizon 2020
844 Marie Skłodowska-Curie Actions individual fellowship (897408). M.W. was supported by a
845 Fulbright grant for Visiting Scholars from the Commission for Educational Exchange between the
846 United States of America, Belgium and Luxembourg. We thank André Bleich, Hannover Medical
847 School, Germany for providing *Il10*$^{-/-}$ mice germ-free mice used in the germ-free facility in
848 Luxembourg. We thank Leonard Augenlicht at Albert Einstein University for sharing conventional
849 Muc2$^{+/-}$ mice.

850

851 **Competing interest statement**

852 M.S.D. works as a consultant and an advisory board member at Theralution GmbH, Germany.

853

854 **Figure Legends**

855 **Figure 1. Low fiber and microbiome driven disease development in *Il10*$^{-/-}$ mice. A.** Weight
856 trajectories of adult C57BL/6J *Il10*$^{-/-}$ mice colonized with the human synthetic microbiota
857 containing 14 species (SM14) and maintained on a fiber rich (FR) diet or switched to a fiber free
858 (FF) diet after 14 d of colonization. Curves represent polynomial (quadratic) equations fit to all
859 of the weight gathered at various days for the two treatments. Weights were measured more
860 frequently after day 40 due to the declining health of the FF group and animals that were
861 euthanized were excluded from the curve at later points. Two FF-fed animals from an early
862 experiment were found dead on arrival and could not be included in subsequent analyses. All
863 others were euthanized if they reached less than 80% starting weight and counted as lethality.

The right axis shows survival in each group over time. The number of mice in each group, along with sexes are indicated in the figure legend. **B.** Representative cecal histology of FF (top) and FR (bottom) fed colonized *Il10*$^{-/-}$ mice. In the top panel, block arrow points to a particularly large ulcer and the line arrow to an area of edema. **C.** Quantitative, blinded histological scoring of cecal tissue taken from colonized *Il10*$^{-/-}$ mice fed the FR and FF diets, along with additional treatments discussed in the text to manipulate individual diet (FR/FF), colonization (SM14 or germfree, latter indicated by dashed lines) and host genotype (wild-type or *Il10*$^{-/-}$*)* variables. Here and in subsequent panels, the red box highlights the condition with most severe inflammation. Bold horizontal bar represents the mean and lighter error bars the S.E.M. **D.** Cecal lipocalin (Lcn2) measurements in the ceca of animal treatments shown in C. Bold horizontal bar represents the mean and lighter error bars the S.E.M. **E.** Mucus penetrability by 1 um-sized beads in the distal colon of *Il10*$^{-/-}$ and wt mice fed the FR and FF diets. **F.** Distance of 1 um-sized beads from the epithelium. **G.** Weight trajectories of *Il10*$^{-/-}$ mice born to either SM14 or specific pathogen free (SPF) parents and weaned to FR or FF. By 79d post weaning (100d after birth), only the SM14, FF group displays weight loss. Curves represent polynomial (quadratic) equations fit to all of the weight gathered at various days for the two treatments. **H.** Survival curves for 4 separate groups of wild-type (wt) C57bl/6 or *Il10*$^{-/-}$ mice colonized by parental transfer of SM14 bacteria at birth. All groups show 100% survival until 29d post weaning (150d total), except for FF fed mice which experience 100% lethality by 105d. **I.** Fecal Lcn2 measurements over time in SM14 colonized *Il10*$^{-/-}$ pups weaned to FR and FF. FF-fed mice experience progressively increasing levels that are reciprocal with the weight trajectory shown in E. Middle horizontal bars represent the mean and flanking error bars the S.E.M. **J.** Endpoint cecal Lcn2 levels in SM14 and SPF colonized mice. Bold horizontal bar represents the mean and lighter error bars the S.E.M. **K.** Mucus thickness measurements in SM14 and SPF colonized mice. Bars represent the mean and error bars the S.E.M. Sample size is indicated below each treatment group. **L.** Cecal Lcn2 measurements in mice fed versions of the FF diet with glucose replaced by dietary fiber from apple, wheat, oat or soluble starch. Concentrations of each addition are provided below the ingredient. Bold horizontal bar represents the mean and lighter error bars the S.E.M. **M.** Fecal Lcn2 measurements over time in SM14 colonized adult mice, which were shifted to FF at 14d post colonization and then shifted back to FR at either 30d or 40d. For each time point and treatment the mean is shown along with individual points and error bars represent S.E.M. **N.** Endpoint histological evaluation of the cecal tissue from mice shown in

896 **L.** compared to mice maintained on FR or FF. Bold horizontal bar represents the mean and
897 lighter error bars the S.E.M. P values: * ≤ 0.05; ** ≤ 0.01; ** ≤ 0.001; *** ≤ 0.001; **** ≤
898 0.0001; ns = not significant.
899
900 **Figure 2. Mucus integrity is central to diet-induced inflammation development. A.** Cecal
901 lipocalin (Lcn2) measurements in *Il10*$^{-/-}$ mice with full or reduced complexity synthetic
902 microbiota as indicated in the "Colonized" line below each graph: Full 14 species SM ("14"),
903 just the 10 species that do not degrade mucin O-glycans *in vitro* ("10"), or 10 non mucin-
904 degrading species plus individual mucin degraders, *B. thetaiotaomicron* (*Bt*), *B. caccae* (*Bc*), *B.*
905 *intestinhominis* (*Bi*) or *A. muciniphila* (*Am*). Bold horizontal bar represents the mean and lighter
906 error bars the S.E.M. **B.** Cecal histology scores of the same treatment group shown in A. **C.**
907 Mucus thickness measurements of SM10 colonized mice fed the FF diet (gray) compared SM14
908 colonized mice fed wither diet. **D.** Representative histology images of SM10, SM10+*Bt* and
909 SM10+*Am.* **E.** Survival curves of *Il10*$^{-/-}$ and DKO adult mice colonized with the SM14. **F.-I.**
910 Individual endpoint weight loss (F.), Cecal Lcn2 (G.), colon histology (H.) and cecal histology
911 (I.) for SM14-colonized *Il10*$^{-/-}$*Muc2*$^{-/-}$ double knockout (DKO) mice fed the FR or FF diets. In all
912 three panels the mean is shown and error bars represent the S.E.M. H. and I. Show **c**omparison of
913 cecal vs. colon histology scores in *Il10*$^{-/-}$ and DKO mice showing worse disease in the colons of
914 DKO mice.
915
916
917 **Figure 3. Mucolytic bacteria influence the inflammatory pathways of colitis. A.** Lipocalin-2
918 levels in the cecal contents and feces of GF and colonized *Il10*$^{-/-}$ mice (n=4-7, two-way ANOVA
919 and post hoc test with Original FDR method of Benjamini and Hochberg). **B.** Proportion of NK
920 cells among CD3^{-}CD45^{+} cells in the cecum and colon lamina propria of SM10- and SM14-
921 colonized *Il10*$^{-/-}$ mice (n=4-11, two-way ANOVA and post hoc test with Original FDR method of
922 Benjamini and Hochberg). **C.** Proportion of CD3^{+}CD4^{+} cells among CD45^{+} cells in the cecum and
923 colon of SM10- and SM14-colonized *Il10*$^{-/-}$ mice (n=4-11, two-way ANOVA and post hoc test
924 with Original FDR method of Benjamini and Hochberg). **D.** Proportion of CD3^{+}CD8^{+} cells among
925 CD45^{+} cells in the cecum and colon of SM10- and SM14-colonized *Il10*$^{-/-}$ mice (n=4-11, two-way
926 ANOVA and post hoc test with Original FDR method of Benjamini and Hochberg). **E.-F.**
927 Proportion of helper T (Th) cell subsets among CD45^{+} cells in the (E) cecum and (F) colon of
928 SM10- and SM14-colonized *Il10*$^{-/-}$ mice (n=4-11, two-way ANOVA and post hoc test with

929 Original FDR method of Benjamini and Hochberg). **G.** Cytokine mRNA levels in the Mesenteric
930 Lymph Nodes (MLN) of *Il10*$^{-/-}$ mice (n=4-11, two-way ANOVA and post hoc test with Original
931 FDR method of Benjamini and Hochberg). **H.** Proportion of regulatory T cell subsets among
932 CD45^{+} cells in the colon of SM10- and SM14-colonized *Il10*$^{-/-}$ mice (n=4-11, two-way ANOVA
933 and post hoc test with Original FDR method of Benjamini and Hochberg). Data are represented as
934 mean ± SD. *p < 0.05; **p < 0.01; ***p < 0.001; ****p < 0.0001.
935
936
937 **Figure 4. Fiber deprivation alters IgA–bacteria interactions in a microbial species-specific**
938 **manner. A.** Concentration of free IgA in the cecal content and feces of GF and colonized *Il10*$^{-/-}$
939 mice (n=4-9, two-way ANOVA and post hoc test with Original FDR method of Benjamini and
940 Hochberg). **B.** Proportion of IgA-producing cells among CD3^{-}CD45^{+} cells in the cecum (left) and
941 colon (right) of GF SM10- and SM14-colonized *Il10*$^{-/-}$ and WT mice (n=4-11, two-way ANOVA
942 and post hoc test with Original FDR method of Benjamini and Hochberg). **C.** IgA-coating profiles
943 of fecal bacteria from SM14-colonized mice fed a FR (top) or a FF (bottom) diet for 56 days
944 showing the gating strategy of population being low-coted (IgA^{low}) and high-coated (IgA^{high}).
945 Total IgA coating showed in panels **D.-E.** consist of the addition of IgA^{high} and IgA^{low} coating. (D)
946 Percentages of total (left), IgA^{high} (middle) and IgA^{low} (right) -coated bacteria as shown in (C) in
947 the feces of FR- and FF-fed, SM14-colonized mice at 21, 56 and 79dpw (n=5-13, two-way
948 ANOVA and post hoc test with the two-stage linear step-up procedure of Benjamini, Krieger and
949 Yekutieli). (E) Percentages of total (left), IgA^{high} (middle) and IgA^{low} (right) -coated bacteria as
950 shown in (C) in the feces of SM10-, SM14- or SPF-colonized *Il10*$^{-/-}$ mice and SM14-colonized
951 WT mice fed the FR or the FF diet for 79 days (n=5-8, two-way ANOVA and post hoc test with
952 the two-stage linear step-up procedure of Benjamini, Krieger and Yekutieli). **F.** IgA-coating index
953 (Kau index) of fecal bacteria from SM14-colonized *Il10*$^{-/-}$ and WT mice (n=2-5, two-way ANOVA
954 and post hoc test with Original FDR method of Benjamini and Hochberg). Data are represented as
955 mean ± SD. *p < 0.05; **p < 0.01; ***p < 0.001; ****p < 0.0001.
956
957 **Figure 5. Co-housing SPF mice with SM14 colonized mice after weaning worsens disease in**
958 **SPF mice. A.** Cecal lipocalin (Lcn2) levels in co-housed or non-co-housed SPF and SM14 mice
959 (co-housing status is indicated at the bottom of this and subsequent panels as appropriate). **B.**
960 Cecal histology of the same treatments shown in A. **C.** Cecal Lcn2 over time in co-housed and
961 non-co-housed SPF and SM14 mice demonstrating inflammatory response starting between 60-

962 80d. Note the difference in the group born SPF when co-housed or not and shown in solid or
963 dashed purple lines. **D.** Correlation of cecal Lcn2 and cecum histology scores of co-housed
964 SM14/SPF fed FF diet showing similarity between these two measurements in individuals. **E.-G.**
965 Relative abundance of SM14 species invading SPF co-housed mice, *E. coli*, *A. muciniphila*, *B.*
966 *intestinihominis*, respectively.
967
968 **Figure 6. A fiber free exclusive enteral nutrition (EEN) diet improves inflammation in part**
969 **through isobutyrate production. A.** Weight trajectories of mice fed low FR, FF, EEN and FF-
970 soy diets. **B.** Cecal lipocalin levels of mice weaned onto FF, FR, and EEN diets. **C.** Cecal histology
971 scores of the same mice shown in B. **D.** Mucus thickness measurements in mice shown in B. and
972 C. revealing that the EEN diet does promote mucus thinning despite dampening disease. **E.** Short-
973 chain fatty acid and isobutyrate measuements in mice fed FF, FR, or EEN diets, inset shows
974 isobutyrate produced levels on a smaller scale. **F.** Inversse correlation between isobutyrate
975 production and Lcn2 levels. **G.** Weight trajectories of mice fed the FF diet and water supplemented
976 with either 35mM isobutyrate (orange) or butyrate (purple), or the FF-soy diet (dark yellow). **H.**
977 Cecal Lcn2 levels in the mice from panel G. **I.** Cecal histology scores of the mice shown in G. **J.**
978 SM14 community composition in mice fed the FR, FF and EEN diets. Note the similarity of
979 preweaned mice to adults fed FF and the 250-fold increase in E. rectale after feeding the EEN diet.
980 **K.** Branched chain fatty acid measurements (isoabutyrate, isovalerate and -methyl butyrate) using
981 LC-MS in culture supernatants of indvidual SM14 bacteria. **L.** Cecal isobutyrate measurements in
982 FF-soy fed mice comparing to measurements from FR, FF and EEn mice shown in panel E. **M.**
983 Correlation plot of Lcn2 and isobutyrate measurements in FF-soy fed mice.
984
985 **Supplemental Figure Legends**
986
987 **Supplemental Figure 1. Low fiber and microbiome driven disease development in *Il10*$^{-/-}$**
988 **mice. A.-C.** Representative histology from wild-type SM14-colonized mice fed FR (A.), wild-
989 type SM14-colonized mice fed FF (B.) or Wild-type germfree mice fed FF (C.). All pictures are
990 shown at 4x magnification. **D.** Endpoint weights of the mice shown in Fig. 1A. Bold horizontal
991 bar represents the mean and lighter error bars the S.E.M. **E.-F.** Relative abundance streamplots
992 of SM14 bacteria in *Il10*$^{-/-}$ (E.) or wild-type (F.) mice shifted to the FF diet at 14d after
993 colonization. Dots below the graph indicate the time points at which feces was sampled and the

994 black bar on the x axis represents the period of FR feeding. **G.** Comparison of cecal *E. coli* and
995 *B. thetaiotaomicron* populations in *Il10*$^{-/-}$ vs wild-type mice after 60d of colonization. Bold
996 horizontal bar represents the mean and lighter error bars the S.E.M. **H.-I.** Representative staining
997 and imaging for Muc2 (green) in colonic sections from FR (H.) or FF (I.) and counter-stained
998 with DAPI (blue). These images were used for automated mucus measurement using BacSpace
999 software as described in methods. **J.** Automated mucus thickness measurements generated from
1000 colonic section images like those shown in H.-I. Five mice were measured per treatment, with a
1001 total of 1-2 fecal mass sections imaged per mouse. **K.** Averaged Muc2 staining intensity
1002 measurements for the mice represented in H.-J. as a function of distance from the epithelium. **L.-**
1003 **M.** Representative visualization of 1um-sized beads (in red) layered on the distal colon
1004 epithelium (in green) after feeding FR (L.) or FF (M.). The space between the beads represents
1005 the mucus layer. **N.** Representative SM14 composition in adult mice fed FR at 13d post gavage
1006 (p.g.) compared to still suckling pups at 14d post birth (p.b.) and 100d old SM14 colonized pups
1007 that were weaned onto either FR or FF diets. **O.** Survival plot of SM14 or SPF colonized pups
1008 weaned onto FR or FF diets and maintained for a total of 100d, the typical experimental duration.
1009 **P.** Cecal histology scores for SM14 or SPF colonized pups weaned onto FR or FF diets and
1010 maintained for a total of 100d. P. Cecal histology scores for SM14 or SPF colonized pups
1011 weaned onto FR or FF diets. Bold horizontal bar represents the mean and lighter error bars the
1012 S.E.M. Related to main text Figure 1.
1013
1014 **Supplemental Figure 2. Fiber supplementation reduces inflammation severity. A.** Endpoint
1015 weights of mice fed variations of the FF diet with glucose replaced by fiber from apple, oat or
1016 wheat, or soluble starch at 7.5% and 44%. Fiber or starch were added at the concentrations listed
1017 below each treatment and an equal amount of glucose was omitted. Bold horizontal bar
1018 represents the mean and lighter error bars the S.E.M. **B.** Cecal histology scores of the treatment
1019 groups shown in A. **C.-F.** Relative abundance streamplots of the SM14 bacteria in *Il10*$^{-/-}$ mice
1020 fed fiber-enriched versions of the FF diet and containing either no added fiber (C.) or purified
1021 fiber from apple (D.), oat (E.) or wheat (F.). **G.** Relative abundance comparison of all 4 mucus
1022 degaders compared to the fiber-degrader *B. ovatus* in adult mice colonized with SM14 and fed
1023 FF or the fiber supplemented diets. Note that the apple diet which had the lowest inflammation
1024 had the largest increase in *B. ovatus* and the largest decrease in mucin degrading bacteria.
1025 Related to main text Figure 1.

1026 **Supplemental Figure 3. Elimination of fiber degrading bacteria reduces inflammation**
1027 **development. A.** Representative mucus staining for SM10 colonized mice used to measure
1028 thickness with Bacspace software. α-Muc2: green, DAPI: blue, prediction of epithelium/mucus
1029 interface: teal. **B.-G.** Relative abundance streamplots of the SM14 IL-10$^{-/-}$ mice all bacteria
1030 present (A.), SM10 (C.), SM10 + *A. muciniphila* (D.), SM10 + *B. caccae* (E.), SM10 + *B.*
1031 *thetaiotaomicron* (F.), SM10 + *B. intestinihominis* (G.). **H.** Weight trajectories of SM14 and
1032 SM10 colonized *Il-10*$^{-/-}$ mice reproduced in a seprate laboratory (LoH). **I.** Endpoint weight of
1033 individual animals shown in H. **J.-O.** Cytokine measurements by Luminex bead assay for wild-
1034 type and *Il-10*$^{-/-}$ mice with various colonization and diet treatment shown in main text Figure 1.
1035 **P-Y.** Cytokine mRNA expression in the cecum of *Il10*$^{-/-}$ pups fed FF or FR diets. (n=4-11, two-
1036 way ANOVA and post hoc test with Original FDR method of Benjamini and Hochberg). Data
1037 are represented as mean ± SD. *p < 0.05; **p < 0.01; ***p < 0.001; ****p < 0.0001.
1038
1039 **Supplemental Figure 4. Fiber deprivation does not cause colitis in the absence of genetic**
1040 **predisposition and the microbiota.** (**A.-B.**) Proportion of immune cell populations in the cecum
1041 and colon of (A.) SM14-colonized WT mice and (B.) GF *Il10*$^{-/-}$ mice (n=5-9, two-way ANOVA
1042 and post hoc test with Original FDR method of Benjamini and Hochberg). Data are represented as
1043 mean ± SD and. For each cell population, data were analyzed along with data from Fig. 3 and S5.
1044 *p < 0.05; **p < 0.01; ***p < 0.001; ****p < 0.0001.
1045
1046 **Supplemental Figure 5. Mucolytic bacteria influence the inflammatory pathways of colitis in**
1047 **an organ-specific manner. A.** Gating Strategy for the analysis of T cells and NK cells in the cecal
1048 and colonic lamina propria. **B.** Proportion of CD3^{+} cells among CD45^{+} cells in the cecum and
1049 colon of SM10- and SM14-colonized *Il10*$^{-/-}$ mice (n=4-11, two-way ANOVA and post hoc test
1050 with Original FDR method of Benjamini and Hochberg). **C.** Cytokine mRNA levels in the
1051 Mesenteric Lymph Nodes (MLN) of *Il10*$^{-/-}$ mice (n=2-11, two-way ANOVA and post hoc test with
1052 Original FDR method of Benjamini and Hochberg). **D.-E.** Proportion of cecal and colonic
1053 regulatory T cells and (D.) and cecal regulatory T cell subsets (E.) among CD45^{+} cells in SM10-
1054 and SM14-colonized *Il10*$^{-/-}$ mice (n=4-11, two-way ANOVA and post hoc test with original FDR
1055 method of Benjamini and Hochberg). Data are represented as mean ± SD. *p < 0.05; **p < 0.01;
1056 ***p < 0.001; ****p < 0.0001.
1057

1058 **Supplemental Figure 6. Fiber deprivation alters IgA–bacteria interactions. A.-B.** Proportion
1059 of B cells ($B220^+$), plasma cells ($CD138^+$), IgD- and IgG-producing cells among $CD3^-CD45^+$ cells
1060 in the (A.) cecum and (B.) colon of GF, SM10- and SM14-colonized *Il10*$^{-/-}$ and WT mice (n=4-11,
1061 two-way ANOVA and post hoc test with Original FDR method of Benjamini and Hochberg). **C.**
1062 Percentages of total (top), IgA^{high} (middle) and IgA^{low} (bottom) -coated bacteria as shown in (C)
1063 in the feces of SM10-, SM14- or SPF-colonized *Il10*$^{-/-}$ mice and SM14-colonized WT mice fed the
1064 FR or the FF diet for 79 days (n=5-8, two-way ANOVA and post hoc test with the two-stage linear
1065 step-up procedure of Benjamini, Krieger and Yekutieli). Data are represented as mean ± SD. *$p < 0.05$;
1066 **$p < 0.01$; ***$p < 0.001$; ****$p < 0.0001$.
1067
1068

1069 **References**
1070

1071 Adamji, M., and Day, A.S. (2019). An overview of the role of exclusive enteral nutrition for
1072 complicated Crohn's disease. Intest Res *17*, 171-176.
1073

1074 Agrawal, M., Burisch, J., Colombel, J.F., and S, C.S. (2020). Viewpoint: Inflammatory Bowel
1075 Diseases Among Immigrants From Low- to High-Incidence Countries: Opportunities and
1076 Considerations. Journal of Crohn's & colitis *14*, 267-273.
1077

1078 An, G., Wei, B., Xia, B., McDaniel, J.M., Ju, T., Cummings, R.D., Braun, J., and Xia, L. (2007).
1079 Increased susceptibility to colitis and colorectal tumors in mice lacking core 3-derived O-
1080 glycans. The Journal of experimental medicine *204*, 1417-1429.
1081

1082 Barros, L., Ferreira, C., and Veldhoen, M. (2022). The fellowship of regulatory and tissue-
1083 resident memory cells. Mucosal immunology *15*, 64-73.
1084

1085 Bergstrom, K., Fu, J., Johansson, M.E., Liu, X., Gao, N., Wu, Q., Song, J., McDaniel, J.M.,
1086 McGee, S., Chen, W.*, et al.* (2017). Core 1- and 3-derived O-glycans collectively maintain the
1087 colonic mucus barrier and protect against spontaneous colitis in mice. Mucosal immunology *10*,
1088 91-103.
1089

1090 Birchenough, G.M., Nystrom, E.E., Johansson, M.E., and Hansson, G.C. (2016). A sentinel
1091 goblet cell guards the colonic crypt by triggering Nlrp6-dependent Muc2 secretion. Science *352*,
1092 1535-1542.
1093

1094 Boyapati, R., Satsangi, J., and Ho, G.T. (2015). Pathogenesis of Crohn's disease. F1000Prime
1095 Rep *7*, 44.
1096

1097 Caruso, R., Mathes, T., Martens, E.C., Kamada, N., Nusrat, A., Inohara, N., and Nunez, G.
1098 (2019). A specific gene-microbe interaction drives the development of Crohn's disease-like
1099 colitis in mice. Sci Immunol *4*, eaaw4341.
1100

1101 Castro-Dopico, T., Dennison, T.W., Ferdinand, J.R., Mathews, R.J., Fleming, A., Clift, D.,
1102 Stewart, B.J., Jing, C., Strongili, K., Labzin, L.I.*, et al.* (2019). Anti-commensal IgG Drives
1103 Intestinal Inflammation and Type 17 Immunity in Ulcerative Colitis. Immunity *50*, 1099-1114
1104 e1010.
1105

1106 David, L.A., Maurice, C.F., Carmody, R.N., Gootenberg, D.B., Button, J.E., Wolfe, B.E., Ling,
1107 A.V., Devlin, A.S., Varma, Y., Fischbach, M.A.*, et al.* (2014). Diet rapidly and reproducibly
1108 alters the human gut microbiome. Nature *505*, 559-563.
1109

1110 Day, A.S., and Lopez, R.N. (2015). Exclusive enteral nutrition in children with Crohn's disease.
1111 World J Gastroenterol *21*, 6809-6816.
1112

1113 Desai, M.S., Seekatz, A.M., Koropatkin, N.M., Kamada, N., Hickey, C.A., Wolter, M., Pudlo,
1114 N.A., Kitamoto, S., Terrapon, N., Muller, A.*, et al.* (2016). A Dietary Fiber-Deprived Gut
1115 Microbiota Degrades the Colonic Mucus Barrier and Enhances Pathogen Susceptibility. Cell
1116 *167*, 1339-1353 e1321.

1117 Earle, K.A., Billings, G., Sigal, M., Lichtman, J.S., Hansson, G.C., Elias, J.E., Amieva, M.R.,
1118 Huang, K.C., and Sonnenburg, J.L. (2015). Quantitative Imaging of Gut Microbiota Spatial
1119 Organization. Cell Host Microbe *18*, 478-488.
1120
1121 Fort, M.M., Leach, M.W., and Rennick, D.M. (1998). A role for NK cells as regulators of CD4+
1122 T cells in a transfer model of colitis. J Immunol *161*, 3256-3261.
1123
1124 Fu, J., Wei, B., Wen, T., Johansson, M.E., Liu, X., Bradford, E., Thomsson, K.A., McGee, S.,
1125 Mansour, L., Tong, M.*, et al.* (2011). Loss of intestinal core 1-derived O-glycans causes
1126 spontaneous colitis in mice. J Clin Invest *121*, 1657-1666.
1127
1128 Furter, M., Sellin, M.E., Hansson, G.C., and Hardt, W.D. (2019). Mucus Architecture and Near-
1129 Surface Swimming Affect Distinct Salmonella Typhimurium Infection Patterns along the Murine
1130 Intestinal Tract. Cell reports *27*, 2665-2678 e2663.
1131
1132 Gomes-Santos, A.C., Moreira, T.G., Castro-Junior, A.B., Horta, B.C., Lemos, L., Cruz, D.N.,
1133 Guimaraes, M.A., Cara, D.C., McCafferty, D.M., and Faria, A.M. (2012). New insights into the
1134 immunological changes in IL-10-deficient mice during the course of spontaneous inflammation
1135 in the gut mucosa. Clin Dev Immunol *2012*, 560817.
1136
1137 Gunasekera, D.C., Ma, J., Vacharathit, V., Shah, P., Ramakrishnan, A., Uprety, P., Shen, Z.,
1138 Sheh, A., Brayton, C.F., Whary, M.T.*, et al.* (2020). The development of colitis in Il10(-/-) mice
1139 is dependent on IL-22. Mucosal immunology *13*, 493-506.
1140
1141 Guo, C.J., Allen, B.M., Hiam, K.J., Dodd, D., Van Treuren, W., Higginbottom, S., Nagashima,
1142 K., Fischer, C.R., Sonnenburg, J.L., Spitzer, M.H.*, et al.* (2019). Depletion of microbiome-
1143 derived molecules in the host using Clostridium genetics. Science *366*, eaav1282.
1144
1145 Gustafsson, J.K., Ermund, A., Johansson, M.E., Schutte, A., Hansson, G.C., and Sjovall, H.
1146 (2012). An ex vivo method for studying mucus formation, properties, and thickness in human
1147 colonic biopsies and mouse small and large intestinal explants. American journal of physiology
1148 Gastrointestinal and liver physiology *302*, G430-438.
1149
1150 Hooper, L.V., and Macpherson, A.J. (2010). Immune adaptations that maintain homeostasis with
1151 the intestinal microbiota. Nat Rev Immunol *10*, 159-169.
1152
1153 Huus, K.E., Bauer, K.C., Brown, E.M., Bozorgmehr, T., Woodward, S.E., Serapio-Palacios, A.,
1154 Boutin, R.C.T., Petersen, C., and Finlay, B.B. (2020). Commensal Bacteria Modulate
1155 Immunoglobulin A Binding in Response to Host Nutrition. Cell Host Microbe *27*, 909-921 e905.
1156
1157 Huus, K.E., Petersen, C., and Finlay, B.B. (2021). Diversity and dynamism of IgA-microbiota
1158 interactions. Nat Rev Immunol *21*, 514-525.
1159
1160 Kakade, M.L., Thompson, R.D., Engelstad, W.E., Behrens, G.C., Yoder, R.D., and Crane, F.M.
1161 (1976). Failure of soybean trypsin inhibitor to exert deleterious effects in calves. Journal of dairy
1162 science *59*, 1484-1489.
1163

1164 Kau, A.L., Planer, J.D., Liu, J., Rao, S., Yatsunenko, T., Trehan, I., Manary, M.J., Liu, T.C.,
1165 Stappenbeck, T.S., Maleta, K.M., *et al.* (2015). Functional characterization of IgA-targeted
1166 bacterial taxa from undernourished Malawian children that produce diet-dependent enteropathy.
1167 Science translational medicine *7*, 276ra224.
1168
1169 Keubler, L.M., Buettner, M., Hager, C., and Bleich, A. (2015). A Multihit Model: Colitis
1170 Lessons from the Interleukin-10-deficient Mouse. Inflamm Bowel Dis *21*, 1967-1975.
1171
1172 Khan, S., Waliullah, S., Godfrey, V., Khan, M.A.W., Ramachandran, R.A., Cantarel, B.L.,
1173 Behrendt, C., Peng, L., Hooper, L.V., and Zaki, H. (2020). Dietary simple sugars alter microbial
1174 ecology in the gut and promote colitis in mice. Science translational medicine *12*, eaay6218.
1175
1176 Kitamoto, S., Alteri, C.J., Rodrigues, M., Nagao-Kitamoto, H., Sugihara, K., Himpsl, S.D.,
1177 Bazzi, M., Miyoshi, M., Nishioka, T., Hayashi, A., *et al.* (2020). Dietary L-serine confers a
1178 competitive fitness advantage to Enterobacteriaceae in the inflamed gut. Nat Microbiol *5*, 116-
1179 125.
1180
1181 Kozich, J.J., Westcott, S.L., Baxter, N.T., Highlander, S.K., and Schloss, P.D. (2013).
1182 Development of a dual-index sequencing strategy and curation pipeline for analyzing amplicon
1183 sequence data on the MiSeq Illumina sequencing platform. Appl Environ Microbiol *79*, 5112-
1184 5120.
1185
1186 Kudelka, M.R., Hinrichs, B.H., Darby, T., Moreno, C.S., Nishio, H., Cutler, C.E., Wang, J., Wu,
1187 H., Zeng, J., Wang, Y., *et al.* (2016). Cosmc is an X-linked inflammatory bowel disease risk
1188 gene that spatially regulates gut microbiota and contributes to sex-specific risk. Proceedings of
1189 the National Academy of Sciences of the United States of America *113*, 14787-14792.
1190
1191 Logan, M., Gkikas, K., Svolos, V., Nichols, B., Milling, S., Gaya, D.R., Seenan, J.P.,
1192 Macdonald, J., Hansen, R., Ijaz, U.Z., *et al.* (2020). Analysis of 61 exclusive enteral nutrition
1193 formulas used in the management of active Crohn's disease-new insights into dietary disease
1194 triggers. Aliment Pharmacol Ther *51*, 935-947.
1195
1196 Maloy, K.J., and Powrie, F. (2011). Intestinal homeostasis and its breakdown in inflammatory
1197 bowel disease. Nature *474*, 298-306.
1198
1199 Marcobal, A., Barboza, M., Sonnenburg, E.D., Pudlo, N., Martens, E.C., Desai, P., Lebrilla,
1200 C.B., Weimer, B.C., Mills, D.A., German, J.B., *et al.* (2011). Bacteroides in the Infant Gut
1201 Consume Milk Oligosaccharides via Mucus-Utilization Pathways. Cell Host Microbe 10, 507-
1202 14.
1203
1204 Martens, E.C., Lowe, E.C., Chiang, H., Pudlo, N.A., Wu, M., McNulty, N.P., Abbott, D.W.,
1205 Henrissat, B., Gilbert, H.J., Bolam, D.N., *et al.* (2011). Recognition and Degradation of Plant
1206 Cell Wall Polysaccharides by Two Human Gut Symbionts. Plos Biol *9*, e1001221.
1207
1208 Mirkov, M.U., Verstockt, B., and Cleynen, I. (2017). Genetics of inflammatory bowel disease:
1209 beyond NOD2. Lancet Gastroenterol Hepatol *2*, 224-234.

1210 Morgan, X.C., Tickle, T.L., Sokol, H., Gevers, D., Devaney, K.L., Ward, D.V., Reyes, J.A.,
1211 Shah, S.A., LeLeiko, N., Snapper, S.B., *et al.* (2012). Dysfunction of the intestinal microbiome
1212 in inflammatory bowel disease and treatment. Genome biology *13*, R79.
1213
1214 Nakajima, A., Vogelzang, A., Maruya, M., Miyajima, M., Murata, M., Son, A., Kuwahara, T.,
1215 Tsuruyama, T., Yamada, S., Matsuura, M., *et al.* (2018). IgA regulates the composition and
1216 metabolic function of gut microbiota by promoting symbiosis between bacteria. The Journal of
1217 experimental medicine *215*, 2019-2034.
1218
1219 Ng, S.C., Shi, H.Y., Hamidi, N., Underwood, F.E., Tang, W., Benchimol, E.I., Panaccione, R.,
1220 Ghosh, S., Wu, J.C.Y., Chan, F.K.L., *et al.* (2017). Worldwide incidence and prevalence of
1221 inflammatory bowel disease in the 21st century: a systematic review of population-based studies.
1222 Lancet *390*, 2769-2778.
1223
1224 Packey, C.D., and Sartor, R.B. (2009). Commensal bacteria, traditional and opportunistic
1225 pathogens, dysbiosis and bacterial killing in inflammatory bowel diseases. Current opinion in
1226 infectious diseases *22*, 292-301.
1227
1228 Palm, N.W., de Zoete, M.R., Cullen, T.W., Barry, N.A., Stefanowski, J., Hao, L., Degnan, P.H.,
1229 Hu, J., Peter, I., Zhang, W., *et al.* (2014). Immunoglobulin A coating identifies colitogenic
1230 bacteria in inflammatory bowel disease. Cell *158*, 1000-1010.
1231
1232 Pizarro, T.T., Pastorelli, L., Bamias, G., Garg, R.R., Reuter, B.K., Mercado, J.R., Chieppa, M.,
1233 Arseneau, K.O., Ley, K., and Cominelli, F. (2011). SAMP1/YitFc mouse strain: a spontaneous
1234 model of Crohn's disease-like ileitis. Inflamm Bowel Dis *17*, 2566-2584.
1235
1236 Porter, N.T., and Martens, E.C. (2017). The Critical Roles of Polysaccharides in Gut Microbial
1237 Ecology and Physiology. Annual review of microbiology *71*, 349-369.
1238
1239 Pudlo, N.A., Urs, K., Crawford, R., Pirani, A., Atherly, T., Jimenez, R., Terrapon, N., Henrissat,
1240 B., Peterson, D., Ziemer, C., *et al.* (2022). Phenotypic and Genomic Diversification in Complex
1241 Carbohydrate-Degrading Human Gut Bacteria. mSystems *7*, e0094721.
1242
1243 Schloss, P.D., Westcott, S.L., Ryabin, T., Hall, J.R., Hartmann, M., Hollister, E.B., Lesniewski,
1244 R.A., Oakley, B.B., Parks, D.H., Robinson, C.J., *et al.* (2009). Introducing mothur: open-source,
1245 platform-independent, community-supported software for describing and comparing microbial
1246 communities. Appl Environ Microbiol *75*, 7537-7541.
1247
1248 Schroeder, B.O., Birchenough, G.M.H., Stahlman, M., Arike, L., Johansson, M.E.V., Hansson,
1249 G.C., and Backhed, F. (2018). Bifidobacteria or Fiber Protects against Diet-Induced Microbiota-
1250 Mediated Colonic Mucus Deterioration. Cell Host Microbe *23*, 27-40 e27.
1251
1252 Sellon, R.K., Tonkonogy, S., Schultz, M., Dieleman, L.A., Grenther, W., Balish, E., Rennick,
1253 D.M., and Sartor, R.B. (1998). Resident enteric bacteria are necessary for development of
1254 spontaneous colitis and immune system activation in interleukin-10-deficient mice. Infect
1255 Immun *66*, 5224-5231.

1256 Seregin, S.S., Golovchenko, N., Schaf, B., Chen, J., Pudlo, N.A., Mitchell, J., Baxter, N.T.,
1257 Zhao, L., Schloss, P.D., Martens, E.C., *et al.* (2017). NLRP6 Protects Il10-/- Mice from Colitis
1258 by Limiting Colonization of Akkermansia muciniphila. Cell reports *19*, 733-745.
1259
1260 Shan, Y., Lee, M., and Chang, E.B. (2021). The Gut Microbiome and Inflammatory Bowel
1261 Diseases. Annu Rev Med. 73, 455-468.
1262
1263 Shimotoyodome, A., Meguro, S., Hase, T., Tokimitsu, I., and Sakata, T. (2000). Short chain fatty
1264 acids but not lactate or succinate stimulate mucus release in the rat colon. Comp Biochem
1265 Physiol A Mol Integr Physiol *125*, 525-531.
1266
1267 Smith, P.M., Howitt, M.R., Panikov, N., Michaud, M., Gallini, C.A., Bohlooly, Y.M., Glickman,
1268 J.N., and Garrett, W.S. (2013). The microbial metabolites, short-chain fatty acids, regulate
1269 colonic Treg cell homeostasis. Science *341*, 569-573.
1270
1271 Sonnenburg, J.L., Xu, J., Leip, D.D., Chen, C.H., Westover, B.P., Weatherford, J., Buhler, J.D.,
1272 and Gordon, J.I. (2005). Glycan foraging in vivo by an intestine-adapted bacterial symbiont.
1273 Science *307*, 1955-1959.
1274
1275 Steimle, A., De Sciscio, A., Neumann, M., Grant, E.T., Pereira, G.V., Ohno, H., Martens, E.C.,
1276 and Desai, M.S. (2021). Constructing a gnotobiotic mouse model with a synthetic human gut
1277 microbiome to study host-microbe cross talk. STAR Protoc *2*, 100607.
1278
1279 Tachibana, M., Watanabe, N., Koda, Y., Oya, Y., Kaminuma, O., Katayama, K., Fan, Z.,
1280 Sakurai, F., Kawabata, K., Hiroi, T., *et al.* (2020). Ablation of IL-17A leads to severe colitis in
1281 IL-10-deficient mice: implications of myeloid-derived suppressor cells and NO production. Int
1282 Immunol *32*, 187-201.
1283
1284 Tan, J., McKenzie, C., Vuillermin, P.J., Goverse, G., Vinuesa, C.G., Mebius, R.E., Macia, L.,
1285 and Mackay, C.R. (2016). Dietary Fiber and Bacterial SCFA Enhance Oral Tolerance and
1286 Protect against Food Allergy through Diverse Cellular Pathways. Cell reports *15*, 2809-2824.
1287
1288 Taurog, J.D., Maika, S.D., Satumtira, N., Dorris, M.L., McLean, I.L., Yanagisawa, H., Sayad,
1289 A., Stagg, A.J., Fox, G.M., Le O'Brien, A., *et al.* (1999). Inflammatory disease in HLA-B27
1290 transgenic rats. Immunol Rev *169*, 209-223.
1291
1292 Van der Post, S., Jabbar, K.S., Birchenough, G., Arike, L., Akhtar, N., Sjovall, H., Johansson,
1293 M.E.V., and Hansson, G.C. (2019). Structural weakening of the colonic mucus barrier is an early
1294 event in ulcerative colitis pathogenesis. Gut *68*, 2142-2151.
1295
1296 Wang, Y., Su, M.A., and Wan, Y.Y. (2011). An essential role of the transcription factor GATA-3
1297 for the function of regulatory T cells. Immunity *35*, 337-348.
1298
1299 Wohlfert, E.A., Grainger, J.R., Bouladoux, N., Konkel, J.E., Oldenhove, G., Ribeiro, C.H., Hall,
1300 J.A., Yagi, R., Naik, S., Bhairavabhotla, R., *et al.* (2011). GATA3 controls Foxp3(+) regulatory
1301 T cell fate during inflammation in mice. J Clin Invest *121*, 4503-4515.
1302

1303 Yang, B.H., Hagemann, S., Mamareli, P., Lauer, U., Hoffmann, U., Beckstette, M., Fohse, L.,
1304 Prinz, I., Pezoldt, J., Suerbaum, S.*, et al.* (2016). Foxp3(+) T cells expressing RORgammat
1305 represent a stable regulatory T-cell effector lineage with enhanced suppressive capacity during
1306 intestinal inflammation. Mucosal immunology *9*, 444-457.
1307
1308 Zhu, L., Shi, T., Zhong, C., Wang, Y., Chang, M., and Liu, X. (2017). IL-10 and IL-10 Receptor
1309 Mutations in Very Early Onset Inflammatory Bowel Disease. Gastroenterology research *10*, 65-
1310 69.
1311
1312 Zhu, W., Winter, M.G., Spiga, L., Hughes, E.R., Chanin, R., Mulgaonkar, A., Pennington, J.,
1313 Maas, M., Behrendt, C.L., Kim, J.*, et al.* (2020). Xenosiderophore Utilization Promotes
1314 Bacteroides thetaiotaomicron Resilience during Colitis. Cell Host Microbe *27*, 376-388 e378.
1315

Figure 1.

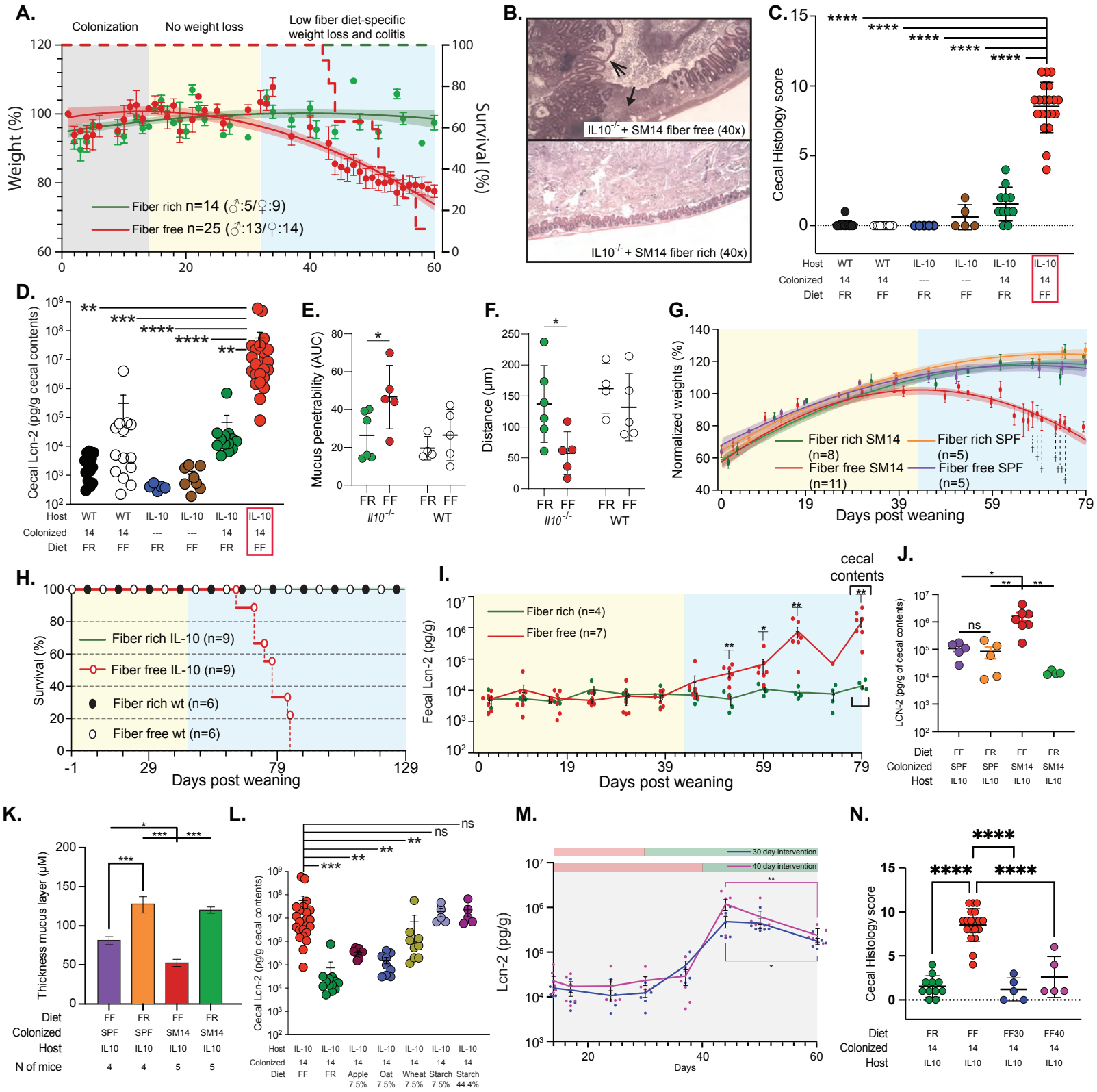
A.
Colonization
No weight loss
Low fiber diet-specific weight loss and colitis
Weight (%)
Survival (%)
Fiber rich n=14 (♂:5/♀:9)
Fiber free n=25 (♂:13/♀:14)
B.
IL10-/- + SM14 fiber free (40x)
IL10-/- + SM14 fiber rich (40x)
C.
Cecal Histology score
Host WT WT IL-10 IL-10 IL-10 IL-10
Colonized 14 14 --- --- 14 14
Diet FR FF FR FF FR FF
D.
Cecal Lcn-2 (pg/g cecal contents)
Host WT WT IL-10 IL-10 IL-10 IL-10
Colonized 14 14 --- --- 14 14
Diet FR FF FR FF FR FF
E.
Mucus penetrability (AUC)
FR FF FR FF
Il10-/- WT
F.
Distance (µm)
FR FF FR FF
Il10-/- WT
G.
Normalized weights (%)
Fiber rich SM14 (n=8)
Fiber free SM14 (n=11)
Fiber rich SPF (n=5)
Fiber free SPF (n=5)
Days post weaning
H.
Survival (%)
Fiber rich IL-10 (n=9)
Fiber free IL-10 (n=9)
Fiber rich wt (n=6)
Fiber free wt (n=6)
Days post weaning
I.
cecal contents
Fecal Lcn-2 (pg/g)
Fiber rich (n=4)
Fiber free (n=7)
Days post weaning
J.
LCN-2 (pg/g of cecal contents)
ns
Diet FF FR FF FR
Colonized SPF SPF SM14 SM14
Host IL10 IL10 IL10 IL10
K.
Thickness mucus layer (µM)
Diet FF FR FF FR
Colonized SPF SPF SM14 SM14
Host IL10 IL10 IL10 IL10
N of mice 4 4 5 5
L.
Cecal Lcn-2 (pg/g cecal contents)
ns
Host IL-10 IL-10 IL-10 IL-10 IL-10 IL-10 IL-10
Colonized 14 14 14 14 14 14 14
Diet FF FR Apple 7.5% Oat 7.5% Wheat 7.5% Starch 7.5% Starch 44.4%
M.
Lcn-2 (pg/g)
30 day intervention
40 day intervention
Days
N.
Cecal Histology score
Diet FR FF FF30 FF40
Colonized 14 14 14 14
Host IL10 IL10 IL10 IL10

Figure 2.

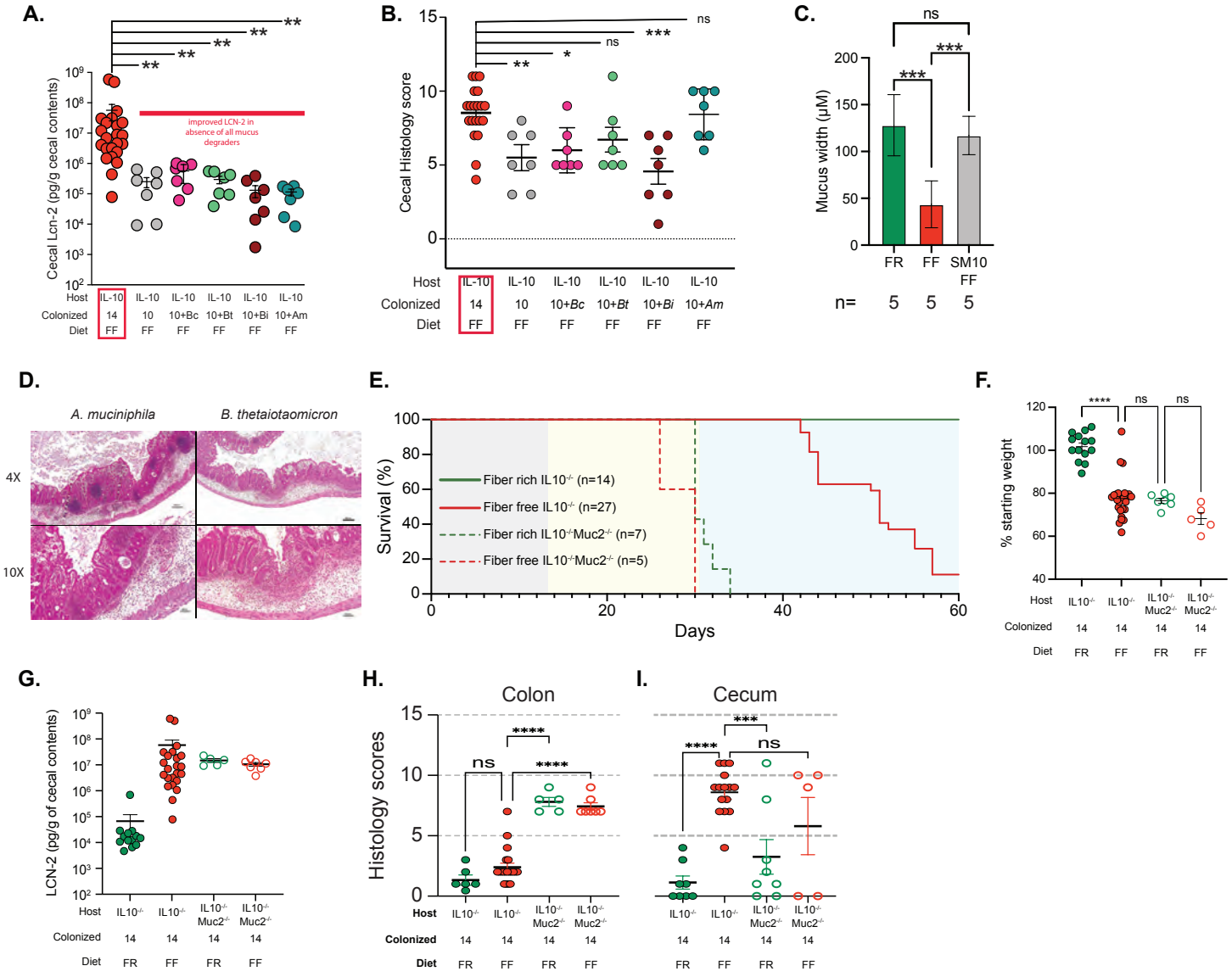
A.
Cecal Lcn-2 (pg/g cecal contents)
improved LCN-2 in absence of all mucus degraders
Host IL-10 IL-10 IL-10 IL-10 IL-10 IL-10
Colonized 14 10 10+Bc 10+Bt 10+Bi 10+Am
Diet FF FF FF FF FF FF
B.
Cecal Histology score
Host IL-10 IL-10 IL-10 IL-10 IL-10 IL-10
Colonized 14 10 10+Bc 10+Bt 10+Bi 10+Am
Diet FF FF FF FF FF FF
C.
Mucus width (µM)
FR FF SM10 FF
n= 5 5 5
D.
A. muciniphila
B. thetaiotaomicron
4X
10X
E.
Survival (%)
Fiber rich IL10-/- (n=14)
Fiber free IL10-/- (n=27)
Fiber rich IL10-/-Muc2-/- (n=7)
Fiber free IL10-/-Muc2-/- (n=5)
Days
F.
% starting weight
Host IL10-/- IL10-/- IL10-/- Muc2-/- IL10-/- Muc2-/-
Colonized 14 14 14 14
Diet FR FF FR FF
G.
LCN-2 (pg/g of cecal contents)
Host IL10-/- IL10-/- IL10-/- Muc2-/- IL10-/- Muc2-/-
Colonized 14 14 14 14
Diet FR FF FR FF
H.
Colon
Histology scores
Host IL10-/- IL10-/- IL10-/- Muc2-/- IL10-/- Muc2-/-
Colonized 14 14 14 14
Diet FR FF FR FF
I.
Cecum
Host IL10-/- IL10-/- IL10-/- Muc2-/- IL10-/- Muc2-/-
Colonized 14 14 14 14
Diet FR FF FR FF

Figure 3

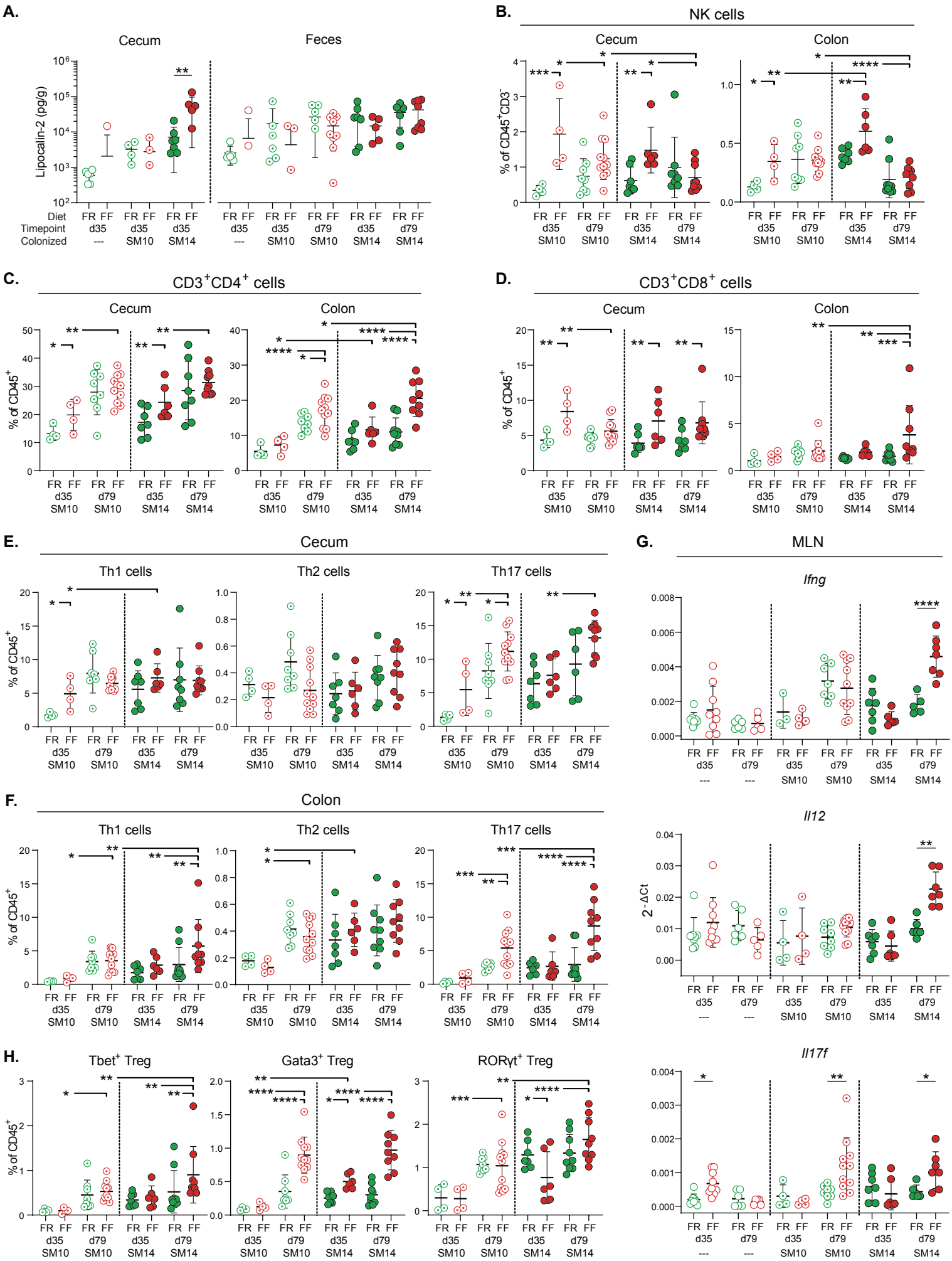
A.
Cecum
Feces
Lipocalin-2 (pg/g)
Diet FR FF FR FF FR FF
Timepoint d35 d35 d35
Colonized --- SM10 SM14
B.
NK cells
Cecum
Colon
% of CD45+CD3-
FR FF FR FF FR FF
d35 d79 d35 d79
SM10 SM10 SM14 SM14
C.
CD3+CD4+ cells
Cecum
Colon
% of CD45+
D.
CD3+CD8+ cells
Cecum
Colon
% of CD45+
E.
Cecum
Th1 cells
Th2 cells
Th17 cells
% of CD45+
F.
Colon
Th1 cells
Th2 cells
Th17 cells
% of CD45+
G.
MLN
Ifng
Il12
Il17f
2-ΔCt
FR FF FR FF FR FF
d35 d79 d35 d79 d35 d79
--- --- SM10 SM10 SM14 SM14
H.
Tbet+ Treg
Gata3+ Treg
RORγt+ Treg
% of CD45+

Figure 4

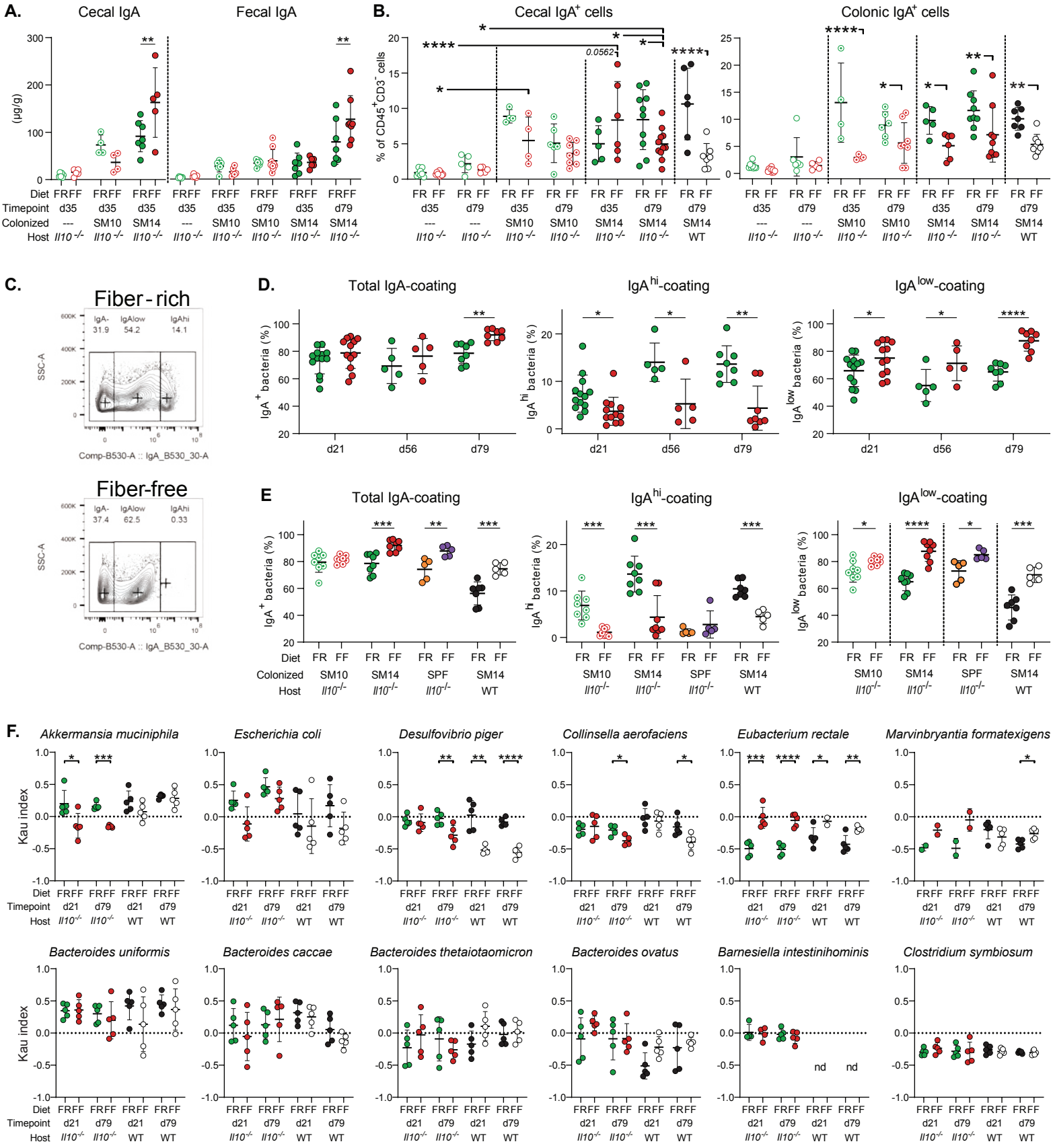
A.
Cecal IgA
Fecal IgA
(µg/g)
Diet FRFF FRFF FRFF FRFF FRFF FRFF FRFF FRFF
Timepoint d35 d35 d35 d35 d35 d79 d35 d79
Colonized --- SM10 SM14 --- SM10 SM10 SM14 SM14
Host Il10 -/- Il10 -/- Il10 -/- Il10 -/- Il10 -/- Il10 -/- Il10 -/- Il10 -/-
B.
Cecal IgA+ cells
Colonic IgA+ cells
% of CD45+CD3- cells
0.0562
FR FF FR FF FR FF FR FF FR FF FR FF FR FF FR FF
d35 d79 d35 d79 d35 d79 d79 d79
--- --- SM10 SM10 SM14 SM14 SM14 SM14
Il10 -/- Il10 -/- Il10 -/- Il10 -/- Il10 -/- Il10 -/- Il10 -/- WT
C.
Fiber-rich
IgA- 31.9
IgAlow 54.2
IgAhi 14.1
SSC-A
Comp-B530-A :: IgA_B530_30-A
Fiber-free
IgA- 37.4
IgAlow 62.5
IgAhi 0.33
D.
Total IgA-coating
IgA+ bacteria (%)
IgAhi-coating
IgAhi bacteria (%)
IgAlow-coating
IgAlow bacteria (%)
d21 d56 d79
E
Total IgA-coating
IgA+ bacteria (%)
IgAhi-coating
IgAhi bacteria (%)
IgAlow-coating
IgAlow bacteria (%)
Diet FR FF FR FF FR FF FR FF
Colonized SM10 SM14 SPF SM14
Host Il10-/- Il10-/- Il10-/- WT
F.
Akkermansia muciniphila
Escherichia coli
Desulfovibrio piger
Collinsella aerofaciens
Eubacterium rectale
Marvinbryantia formatexigens
Bacteroides uniformis
Bacteroides caccae
Bacteroides thetaiotaomicron
Bacteroides ovatus
Barnesiella intestinihominis
Clostridium symbiosum
Kau index
nd nd
Diet FRFF FRFF FRFF FRFF
Timepoint d21 d79 d21 d79
Host Il10-/- Il10-/- WT WT

Figure 5.

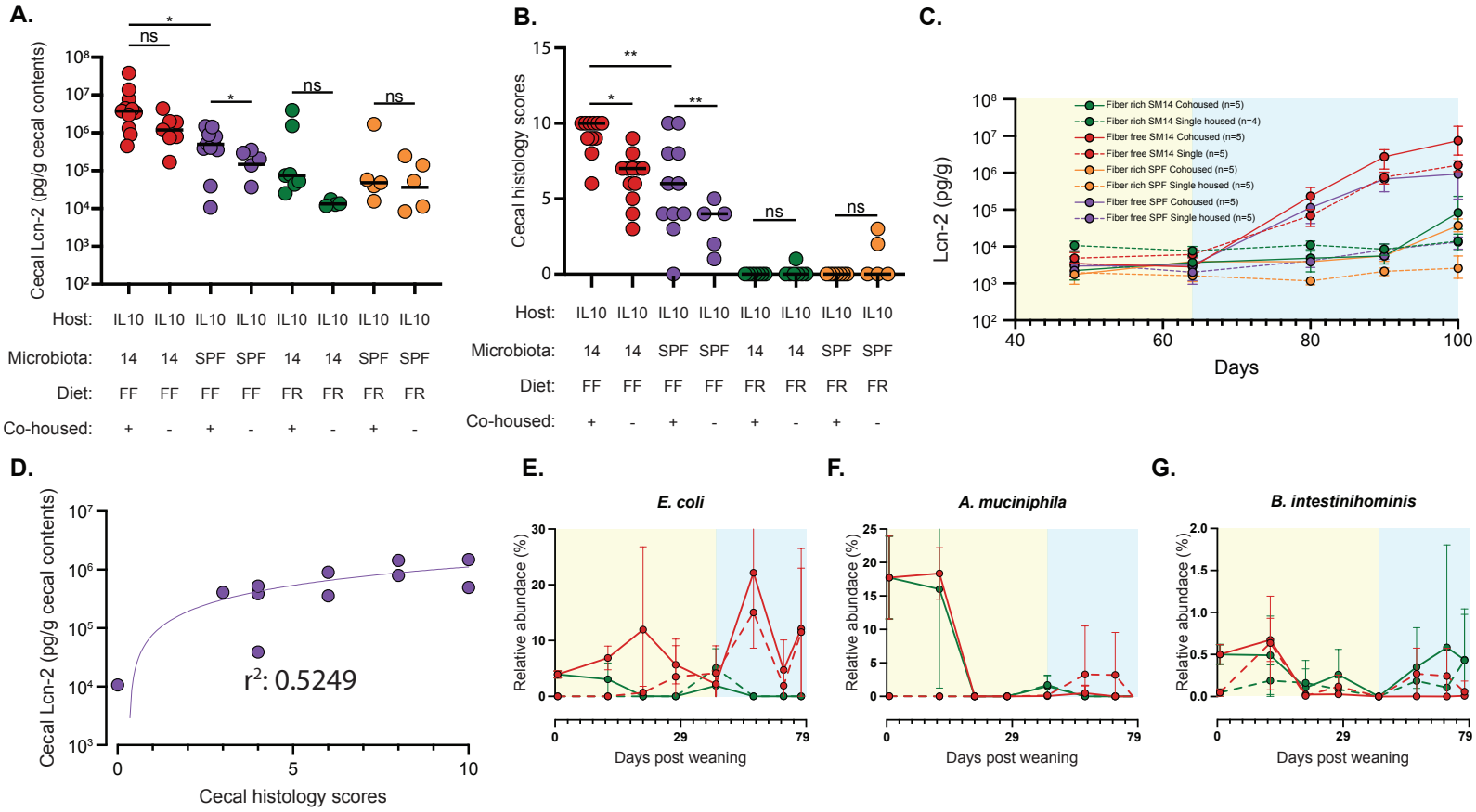
A.
Cecal Lcn-2 (pg/g cecal contents)
Host: IL10 IL10 IL10 IL10 IL10 IL10 IL10 IL10
Microbiota: 14 14 SPF SPF 14 14 SPF SPF
Diet: FF FF FF FF FR FR FR FR
Co-housed: + - + - + - + -
B.
Cecal histology scores
C.
Lcn-2 (pg/g)
Days
Fiber rich SM14 Cohoused (n=5)
Fiber rich SM14 Single housed (n=4)
Fiber free SM14 Cohoused (n=5)
Fiber free SM14 Single (n=5)
Fiber rich SPF Cohoused (n=5)
Fiber rich SPF Single housed (n=5)
Fiber free SPF Cohoused (n=5)
Fiber free SPF Single housed (n=5)
D.
Cecal Lcn-2 (pg/g cecal contents)
r2: 0.5249
Cecal histology scores
E.
E. coli
F.
A. muciniphila
G.
B. intestinihominis
Relative abundace (%)
Days post weaning

Figure 6.

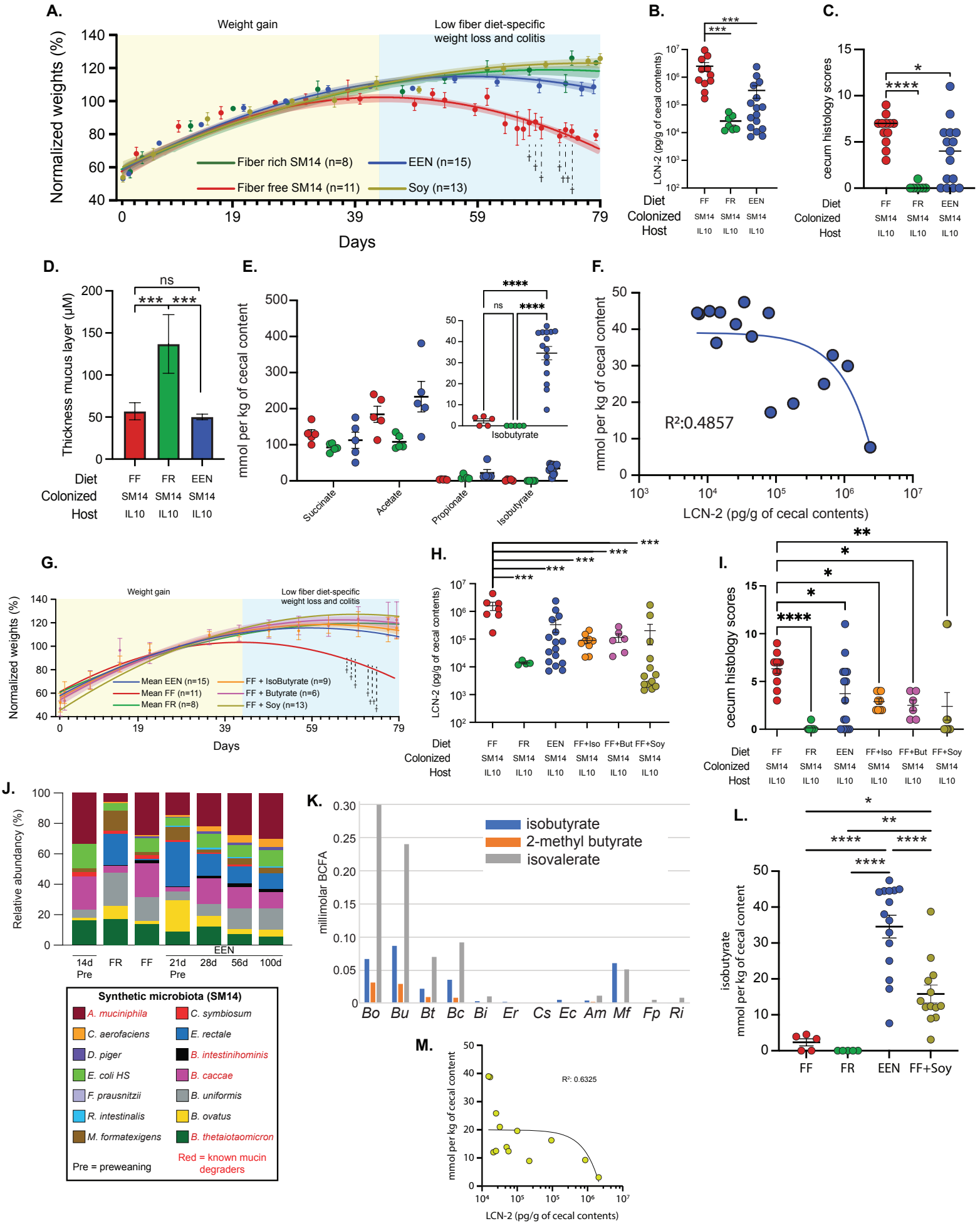
A.
Weight gain
Low fiber diet-specific weight loss and colitis
Normalized weights (%)
Days
Fiber rich SM14 (n=8)
EEN (n=15)
Fiber free SM14 (n=11)
Soy (n=13)
B.
LCN-2 (pg/g of cecal contents)
C.
cecum histology scores
D.
Thickness mucus layer (µM)
ns
E.
mmol per kg of cecal content
Succinate
Acetate
Propionate
Isobutyrate
F.
mmol per kg of cecal content
R²:0.4857
LCN-2 (pg/g of cecal contents)
G.
Weight gain
Low fiber diet-specific weight loss and colitis
Normalized weights (%)
Days
Mean EEN (n=15)
Mean FF (n=11)
Mean FR (n=8)
FF + IsoButyrate (n=9)
FF + Butyrate (n=6)
FF + Soy (n=13)
H.
LCN-2 (pg/g of cecal contents)
I.
cecum histology scores
Diet
Colonized
Host
FF
FR
EEN
FF+Iso
FF+But
FF+Soy
SM14
IL10
J.
Relative abundancy (%)
14d Pre
FR
FF
21d Pre
28d
56d
100d
Synthetic microbiota (SM14)
A. muciniphila
C. symbiosum
C. aerofaciens
E. rectale
D. piger
B. intestinihominis
E. coli HS
B. caccae
F. prausnitzii
B. uniformis
R. intestinalis
B. ovatus
M. formatexigens
B. thetaiotaomicron
Pre = preweaning
Red = known mucin degraders
K.
millimolar BCFA
isobutyrate
2-methyl butyrate
isovalerate
Bo
Bu
Bt
Bc
Bi
Er
Cs
Ec
Am
Mf
Fp
Ri
L.
isobutyrate mmol per kg of cecal content
M.
mmol per kg of cecal content
R²: 0.6325
LCN-2 (pg/g of cecal contents)

Figure S1.

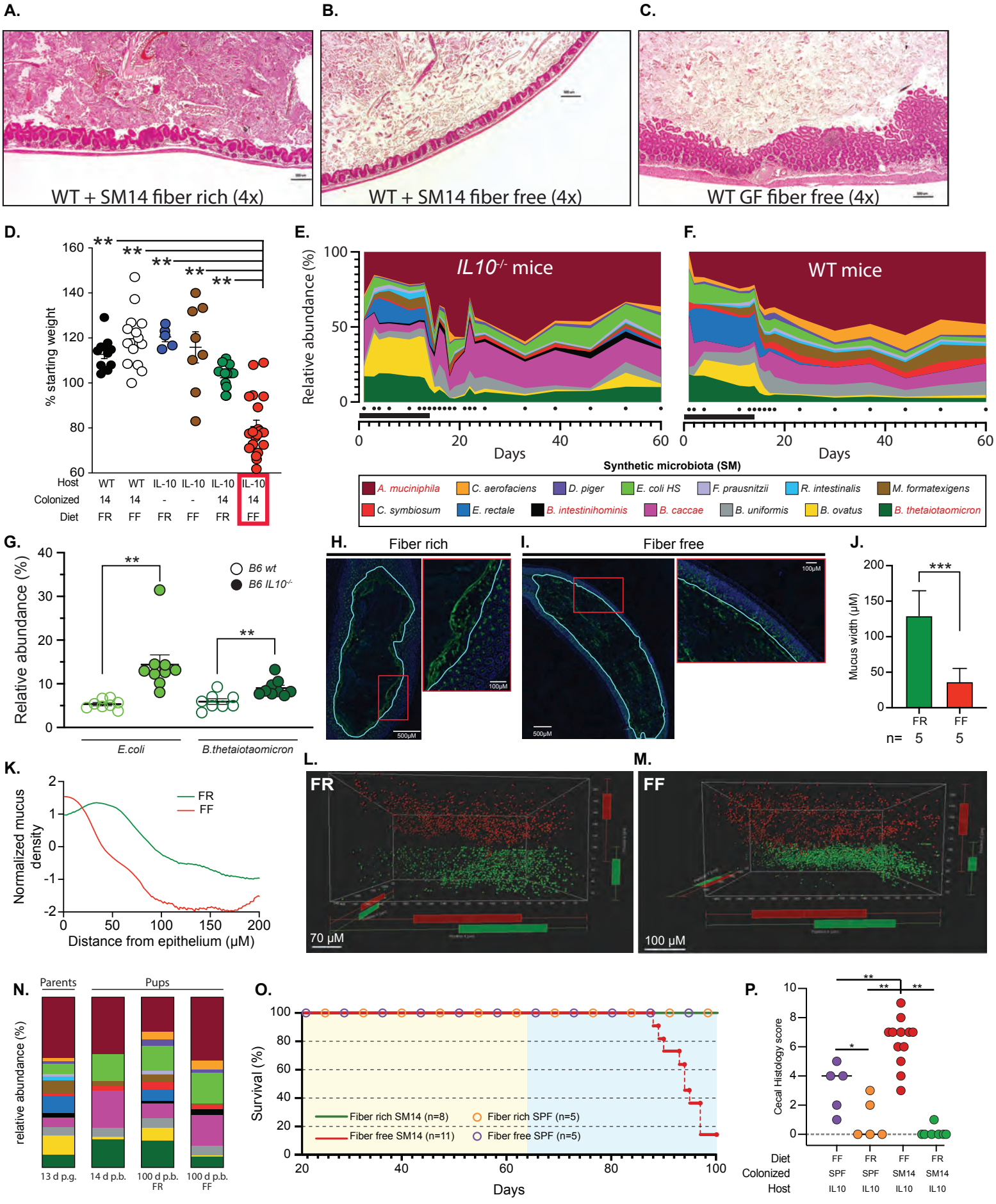
A.
WT + SM14 fiber rich (4x)
B.
WT + SM14 fiber free (4x)
C.
WT GF fiber free (4x)
D.
% starting weight
Host WT WT IL-10 IL-10 IL-10 IL-10
Colonized 14 14 - - 14 14
Diet FR FF FR FF FR FF
E.
IL10-/- mice
Relative abundance (%)
Days
F.
WT mice
Days
Synthetic microbiota (SM)
A. muciniphila
C. aerofaciens
D. piger
E. coli HS
F. prausnitzii
R. intestinalis
M. formatexigens
C. symbiosum
E. rectale
B. intestinihominis
B. caccae
B. uniformis
B. ovatus
B. thetaiotaomicron
G.
Relative abundance (%)
B6 wt
B6 IL10-/-
E.coli
B.thetaiotaomicron
H.
Fiber rich
I.
Fiber free
J.
Mucus width (µM)
FR
FF
n= 5 5
K.
Normalized mucus density
FR
FF
Distance from epithelium (µM)
L.
FR
70 µM
M.
FF
100 µM
N.
Parents
Pups
relative abundance (%)
13 d p.g.
14 d p.b.
100 d p.b. FR
100 d p.b. FF
O.
Survival (%)
Fiber rich SM14 (n=8)
Fiber rich SPF (n=5)
Fiber free SM14 (n=11)
Fiber free SPF (n=5)
Days
P.
Cecal Histology score
Diet FF FR FF FR
Colonized SPF SPF SM14 SM14
Host IL10 IL10 IL10 IL10

Figure S2.

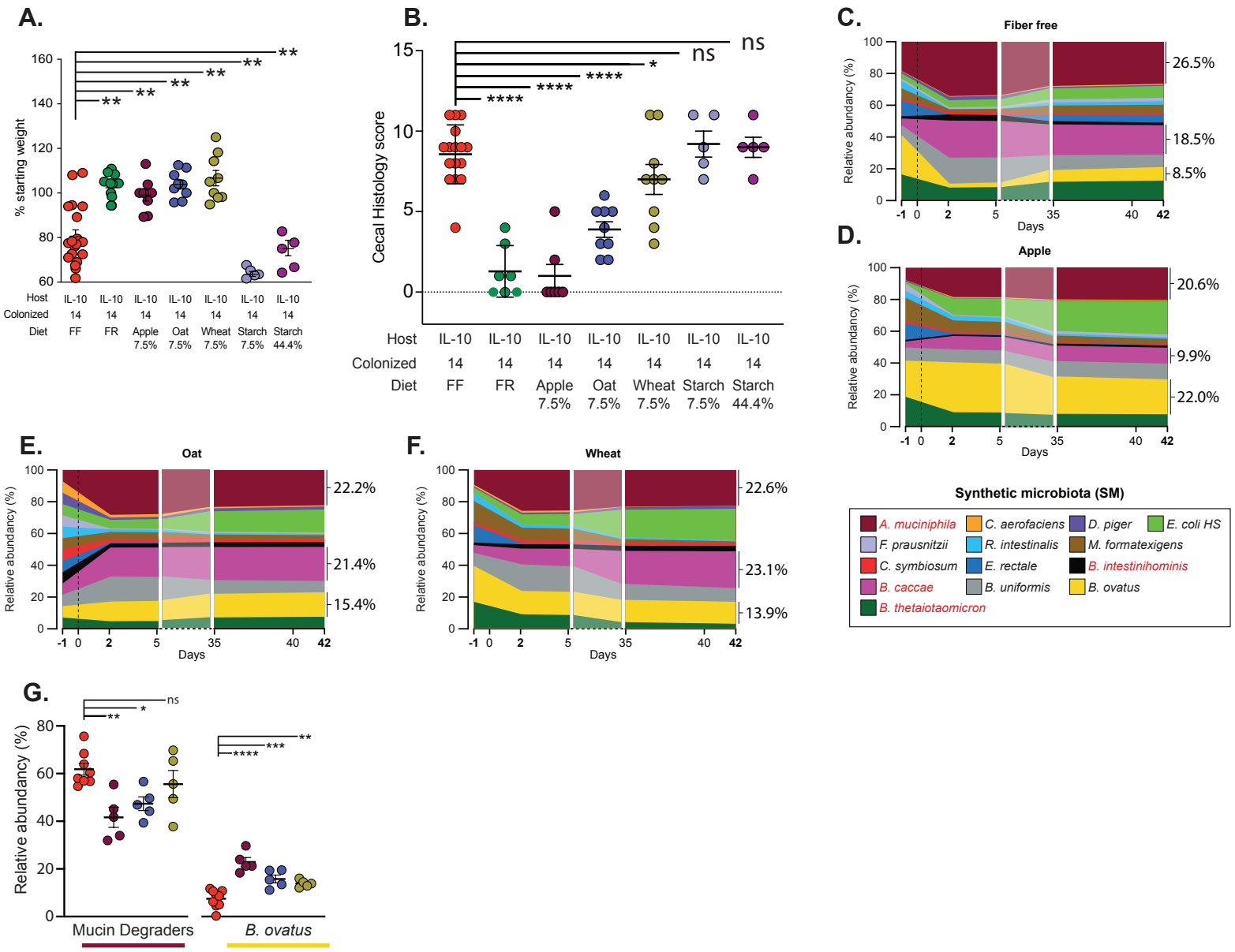
A.
% starting weight
Host
Colonized
Diet
IL-10 14 FF
IL-10 14 FR
IL-10 14 Apple 7.5%
IL-10 14 Oat 7.5%
IL-10 14 Wheat 7.5%
IL-10 14 Starch 7.5%
IL-10 14 Starch 44.4%
B.
Cecal Histology score
ns
C.
Fiber free
Relative abundancy (%)
Days
26.5%
18.5%
8.5%
D.
Apple
20.6%
9.9%
22.0%
E.
Oat
22.2%
21.4%
15.4%
F.
Wheat
22.6%
23.1%
13.9%
Synthetic microbiota (SM)
A. muciniphila
C. aerofaciens
D. piger
E. coli HS
F. prausnitzii
R. intestinalis
M. formatexigens
C. symbiosum
E. rectale
B. intestinihominis
B. caccae
B. uniformis
B. ovatus
B. thetaiotaomicron
G.
Relative abundancy (%)
Mucin Degraders
B. ovatus

Figure S3

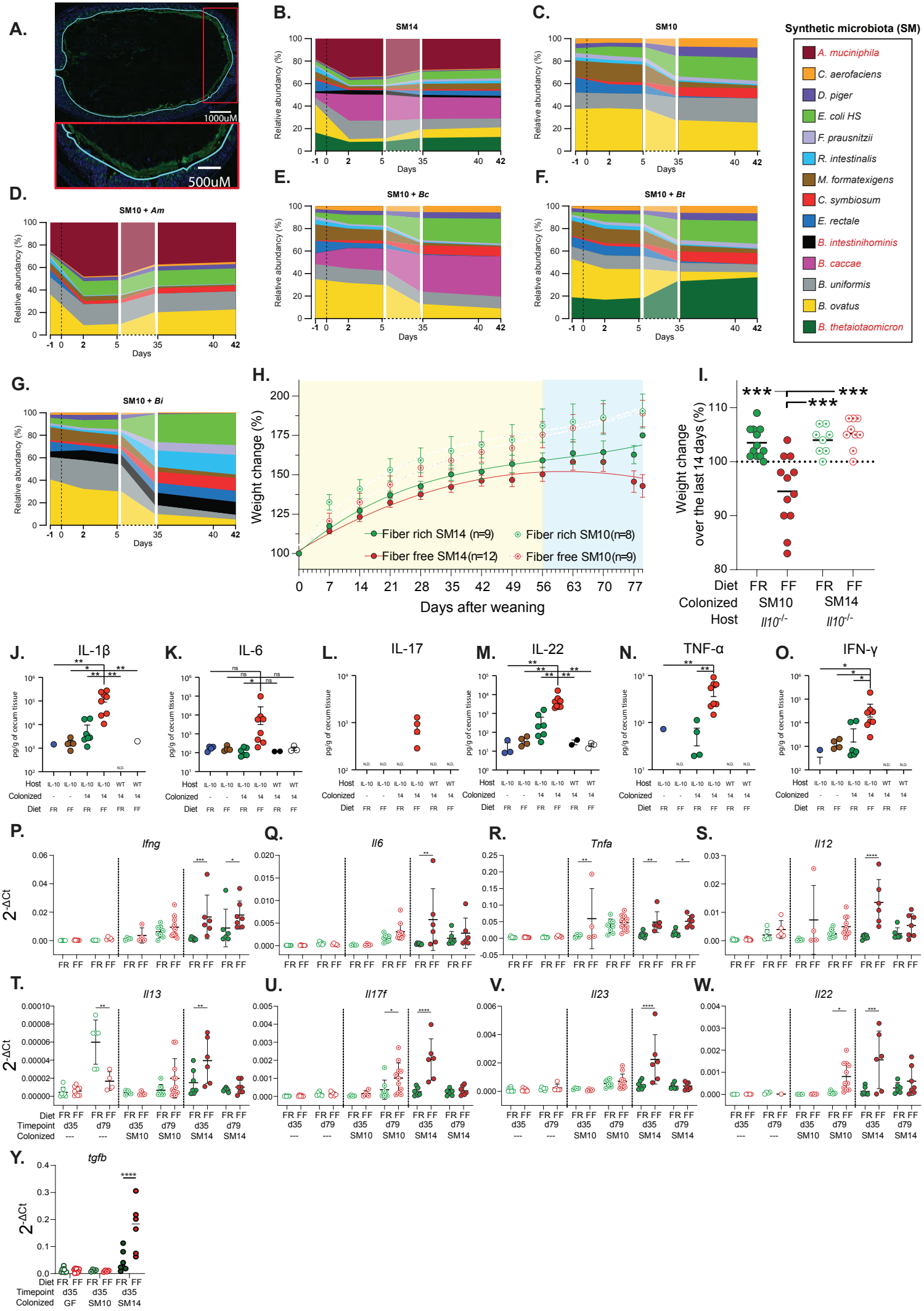
A.
1000uM
500uM
B.
SM14
C.
SM10
D.
SM10 + Am
E.
SM10 + Bc
F.
SM10 + Bt
G.
SM10 + Bi
Relative abundancy (%)
Days
Synthetic microbiota (SM)
A. muciniphila
C. aerofaciens
D. piger
E. coli HS
F. prausnitzii
R. intestinalis
M. formatexigens
C. symbiosum
E. rectale
B. intestinihominis
B. caccae
B. uniformis
B. ovatus
B. thetaiotaomicron
H.
Weight change (%)
Fiber rich SM14 (n=9)
Fiber rich SM10(n=8)
Fiber free SM14(n=12)
Fiber free SM10(n=9)
Days after weaning
I.
Weight change over the last 14 days (%)
Diet
Colonized
Host
SM10
SM14
Il10-/-
J. IL-1β
K. IL-6
L. IL-17
M. IL-22
N. TNF-α
O. IFN-γ
pg/g of cecum tissue
P. Ifng
Q. Il6
R. Tnfa
S. Il12
T. Il13
U. Il17f
V. Il23
W. Il22
2-ΔCt
Timepoint
Y. tgfb

Figure S4

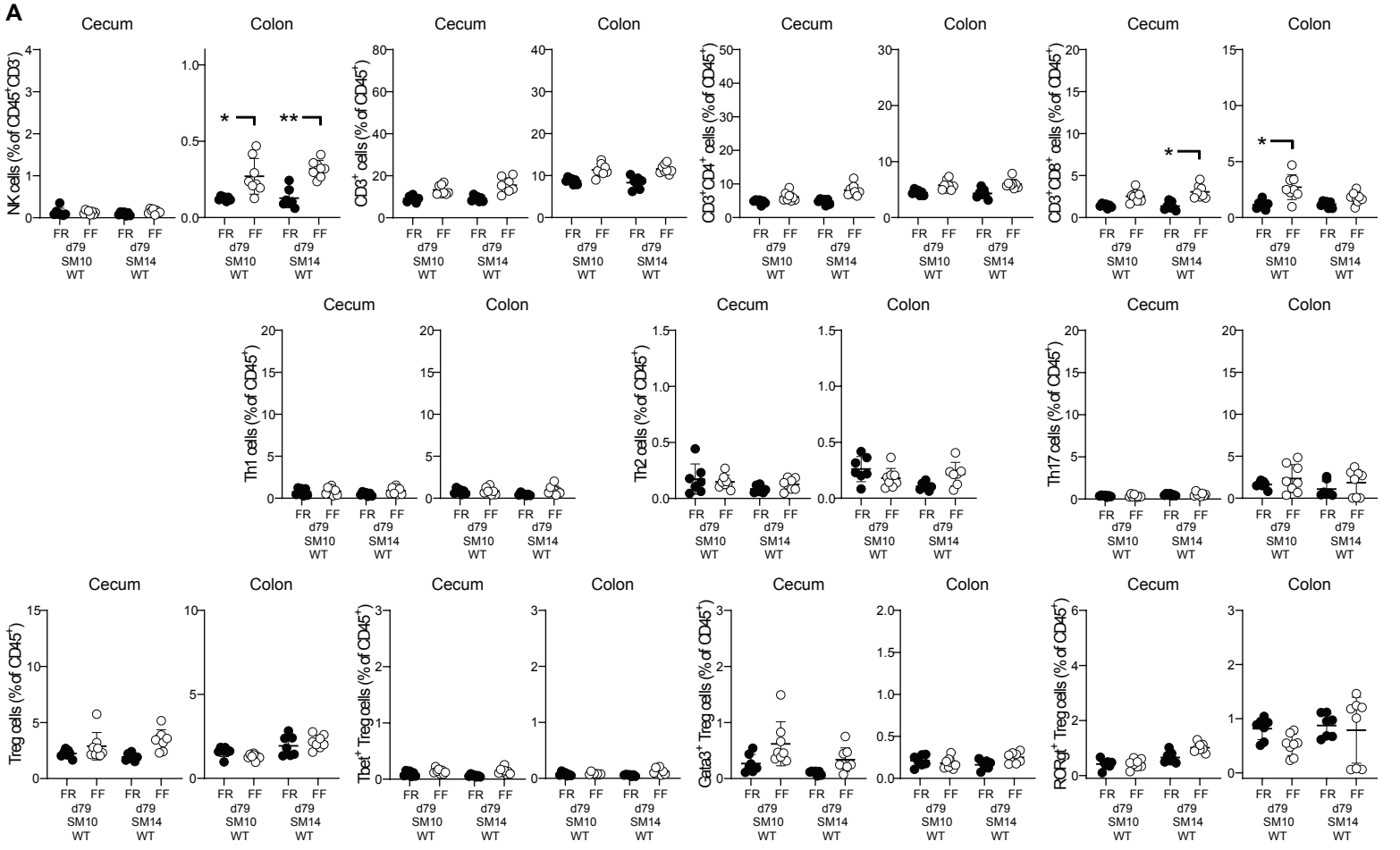
A
Cecum
Colon
NK cells (% of CD45+CD3-)
CD3+ cells (% of CD45+)
CD3+CD4+ cells (% of CD45+)
CD3+CD8+ cells (% of CD45+)
Th1 cells (% of CD45+)
Th2 cells (% of CD45+)
Th17 cells (% of CD45+)
Treg cells (% of CD45+)
Tbet+ Treg cells (% of CD45+)
Gata3+ Treg cells (% of CD45+)
RORγt+ Treg cells (% of CD45+)
FR FF FR FF
d79 d79
SM10 SM14
WT

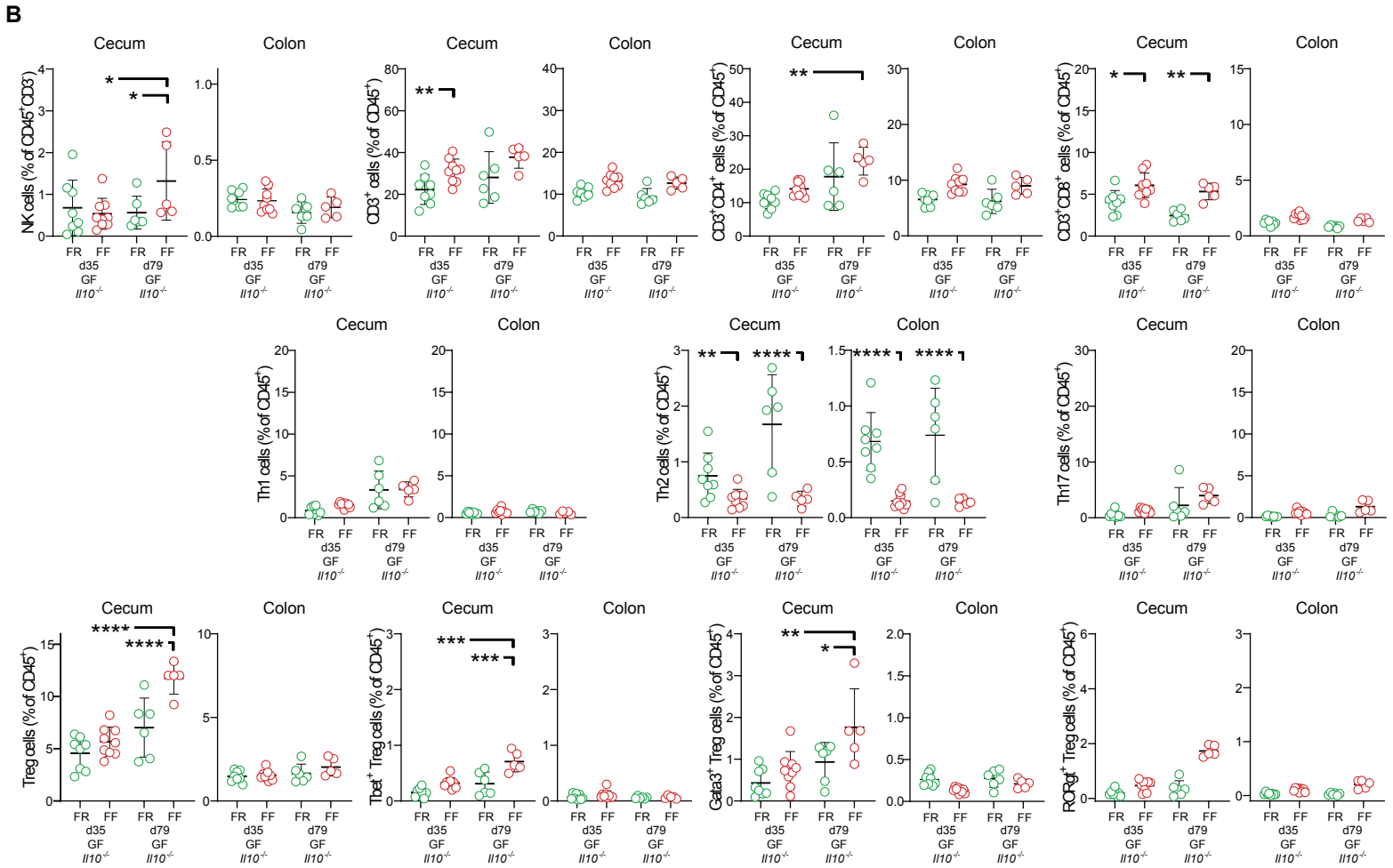
B
Cecum
Colon
NK cells (% of CD45+CD3-)
CD3+ cells (% of CD45+)
CD3+CD4+ cells (% of CD45+)
CD3+CD8+ cells (% of CD45+)
Th1 cells (% of CD45+)
Th2 cells (% of CD45+)
Th17 cells (% of CD45+)
Treg cells (% of CD45+)
Tbet+ Treg cells (% of CD45+)
Gata3+ Treg cells (% of CD45+)
RORγt+ Treg cells (% of CD45+)
FR FF FR FF
d35 d79
GF GF
Il10-/-

Figure S5

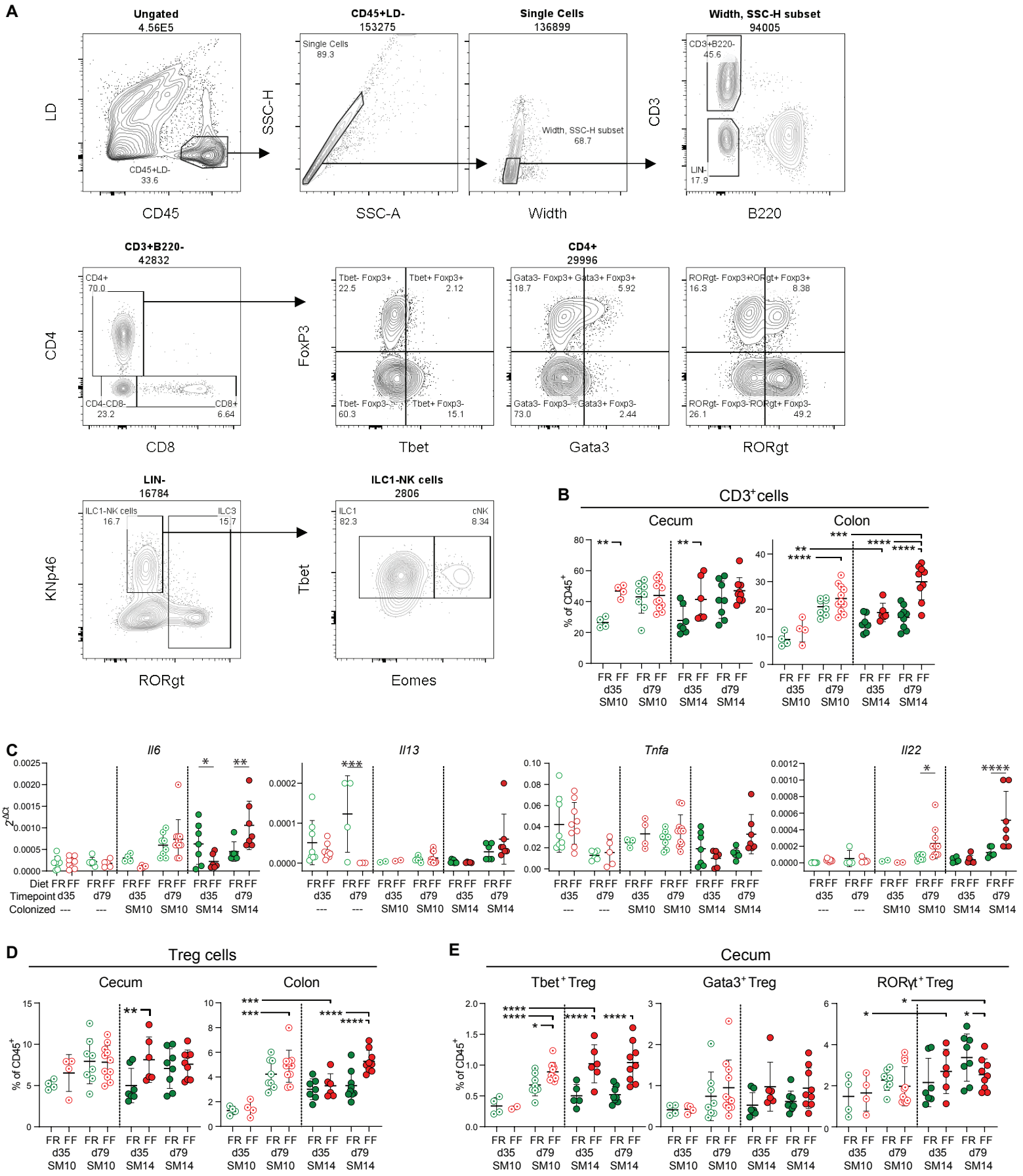
A
Ungated
4.56E5
LD
CD45
CD45+LD-
33.6
CD45+LD-
153275
Single Cells
89.3
SSC-H
SSC-A
Single Cells
136899
Width, SSC-H subset
68.7
Width
Width, SSC-H subset
94005
CD3+B220-
45.6
LIN-
17.9
CD3
B220
CD3+B220-
42832
CD4+
70.0
CD4-CD8-
23.2
CD8+
6.64
CD4
CD8
CD4+
29996
Tbet- Foxp3+
22.5
Tbet+ Foxp3+
2.12
Tbet- Foxp3-
60.3
Tbet+ Foxp3-
15.1
FoxP3
Tbet
Gata3- Foxp3+
18.7
Gata3+ Foxp3+
5.92
Gata3- Foxp3-
73.0
Gata3+ Foxp3-
2.44
Gata3
RORgt- Foxp3+
16.3
RORgt+ Foxp3+
8.38
RORgt- Foxp3-
26.1
RORgt+ Foxp3-
49.2
RORgt
LIN-
16784
ILC1-NK cells
16.7
ILC3
15.7
KNp46
RORgt
ILC1-NK cells
2806
ILC1
82.3
cNK
8.34
Tbet
Eomes
B
CD3+cells
Cecum
Colon
% of CD45+
FR FF
d35 d79
SM10 SM14
C
Il6
Il13
Tnfa
Il22
2ΔCt
Diet FR FF
Timepoint d35 d79
Colonized --- SM10 SM14
D
Treg cells
Cecum
Colon
% of CD45+
E
Cecum
Tbet+ Treg
Gata3+ Treg
RORγt+ Treg
% of CD45+

Figure S6

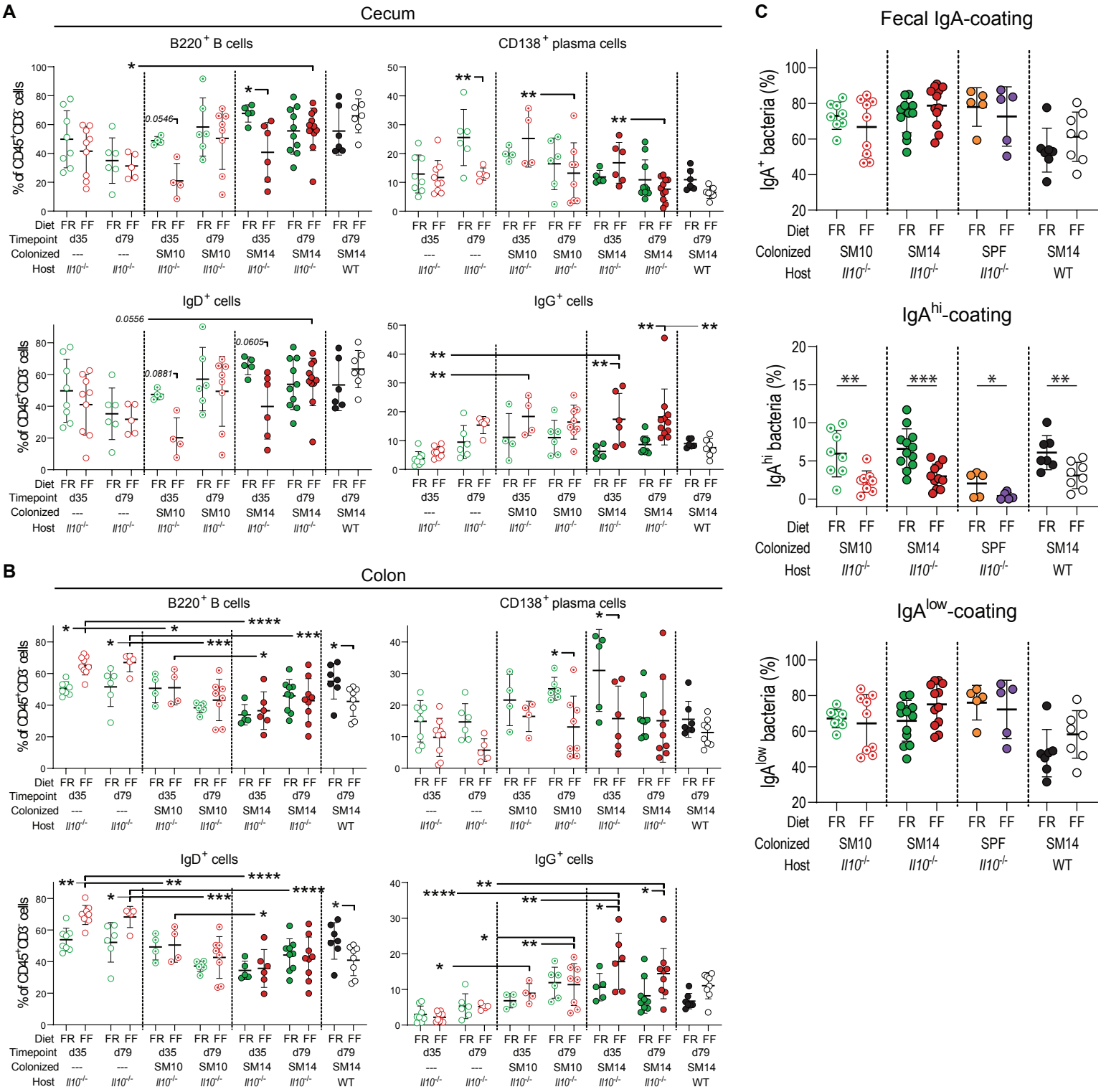
A
Cecum
B220+ B cells
CD138+ plasma cells
IgD+ cells
IgG+ cells
% of CD45+CD3- cells
Diet FR FF FR FF FR FF FR FF FR FF FR FF FR FF
Timepoint d35 d79 d35 d79 d35 d79 d35 d79 d79
Colonized --- --- SM10 SM10 SM14 SM14 SM14
Host Il10-/- Il10-/- Il10-/- Il10-/- Il10-/- Il10-/- WT
0.0546
0.0556
0.0881
0.0605
B
Colon
C
Fecal IgA-coating
IgA+ bacteria (%)
Diet FR FF FR FF FR FF FR FF
Colonized SM10 SM14 SPF SM14
Host Il10-/- Il10-/- Il10-/- WT
IgAhi-coating
IgAhi bacteria (%)
IgAlow-coating
IgAlow bacteria (%)

Figure S7.

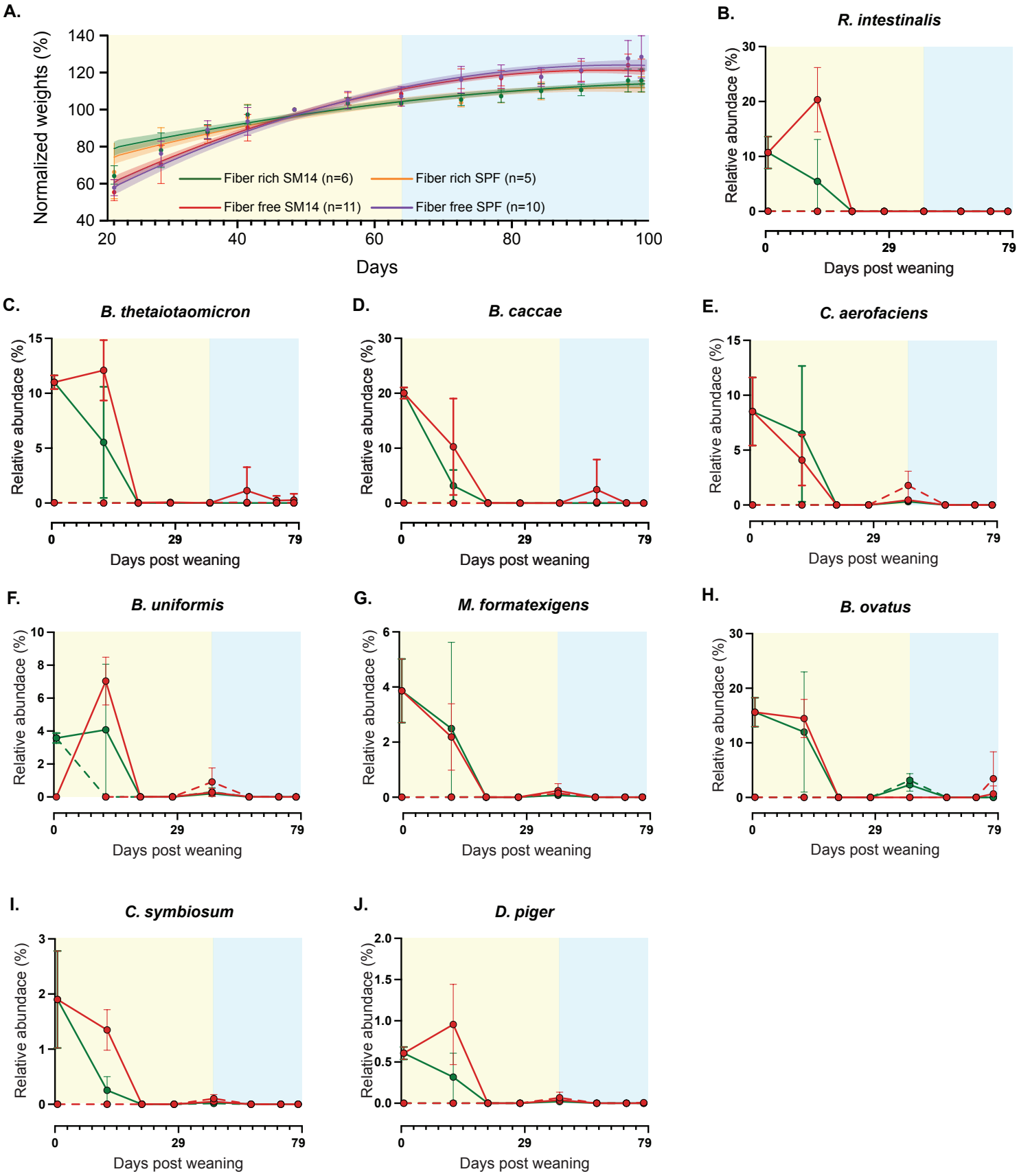
A.
Normalized weights (%)
Days
Fiber rich SM14 (n=6)
Fiber rich SPF (n=5)
Fiber free SM14 (n=11)
Fiber free SPF (n=10)
B.
R. intestinalis
C.
B. thetaiotaomicron
D.
B. caccae
E.
C. aerofaciens
F.
B. uniformis
G.
M. formatexigens
H.
B. ovatus
I.
C. symbiosum
J.
D. piger
Relative abundace (%)
Days post weaning

Table S1. Nutritional and ingredient comparison between fiber free (FF) diet, its soy protein variant, and Exclusive Enteral Nutrition diet Nestle Nutren 1.5

	Fiber free (FF) diet (% kcal from)	Nestle Nutren 1.5 (% kcal from)	Fiber free soy (FF-soy) (% kcal from)
Protein	23.6	18	23.6
Fat	34	35	34
Carbohydrate (total)	42.4	47	42.4
Total:	**100**	**100**	**100**
*Fiber %	8	0	9.6
Accessible fiber%	0	0	1.6
Main ingredients:	glucose (44.4%)	corn syrup (glucose/fructose)	glucose (44.4%)
(Descending order)	casein (26.9%)	maltodextrin	soy protein isolate (26.9%)
	fat from corn oil (7.5%), lard (7.5%)	canola oil	fat from corn oil (7.5%), lard (7.5%)
	cellulose (8%)	soy protein isolate	cellulose (8%)
		sodium caseinate	
		medium chain triglycerides (<2%)	
		calcium caseinate	
	(vitamin, minerals, antioxidants, and stabilizers not shown)	(vitamin, minerals, antioxidants, and stabilizers not shown)	(vitamin, minerals, antioxidants, and stabilizers not shown)

*Note the only fiber added to the FF diet is crystalline cellulose as a bulking agent and is not known be accessible by any SM14 bacteria.